buildings

MDPI

Article

Mechanical Properties and Reproducibility of One-Part Ambient-Cured Slag and Fly Ash-Based Geopolymer Concrete

Daro Sun [1,*], Jessey Lee [1], Alireza Mohyeddin [2] and Janitha Migunthanna [1]

[1] Department of Civil and Construction Engineering, Swinburne University of Technology, Hawthorn, Melbourne, VIC 3122, Australia
[2] School of Engineering, Edith Cowan University, Joondalup, WA 6027, Australia
* Correspondence: darosun@swin.edu.au

Abstract

The cement industry is a major source of anthropogenic CO_2 emissions due to its energy-intensive production process and calcination of limestone. Producing one ton of cement emits approximately one ton of CO_2, and cement accounts for about 5% to 8% of global CO_2 emissions. In this context, cement-less one-part ("just-add-water") ambient-cured geopolymer concrete (GPC) has gained attention due to its environmental friendliness and practicality for large-scale cast-in-situ construction. However, field adoption remains limited, mainly due to the scarcity of data on mechanical properties and durability, as well as the lack of widely accepted standards and specifications. This paper is part of the larger research on tensile performance of anchors embedded in GPC. It is well understood that the tensile performance of anchors installed in concrete substrate is largely influenced by their effective embedment depth and the substrate's mechanical properties, particularly the fracture energy and modulus of elasticity. Therefore, prior to the investigation of the tensile performance of anchors in GPC, it is crucial to understand the mechanical behaviour of the GPC substrate itself. This study examined key parameters that influence the compressive strength of one-part ambient-cured slag/fly ash-based GPC. The alkali content, slag content, water-to-solid (W/S) ratio, and aggregate content were investigated. Additionally, various mechanical properties such as uniaxial tensile strength, splitting tensile strength, elastic modulus, and fracture energy of the hardened GPC are presented. The test results revealed that higher slag and activator content enhanced compressive strength, whereas a higher aggregate content reduced the strength. The strength gain was also attributed to higher alkali content, lower W/S ratio, and increased binder content; however, excessive alkali and an overly low W/S ratio caused rapid setting due to accelerated reaction kinetics. The 7-day compressive strength ranged from 62% to 78% of the 28-day strength, while there was no notable strength gain after 28 days of curing. The developed GPC attained compressive strengths of over 40 MPa at 28 days and 50 MPa at 56 days. The uniaxial tensile strength test demonstrated a ratio of 0.87 relative to splitting tensile strength. The findings also indicated that the aggregate conditions and curing regimes (whether using as-is aggregates with moisture curing or oven-dried aggregates with sealed curing) had no meaningful effect on the mean compressive strength of GPC and its reproducibility.

Keywords: one-part; ambient-cured; geopolymer concrete; fracture energy; uniaxial tensile strength; reproducibility

Check for updates

Academic Editor: Vipul Patel

Received: 15 December 2025
Revised: 31 January 2026
Accepted: 4 February 2026
Published: 9 February 2026

Copyright: © 2026 by the authors. Licensee MDPI, Basel, Switzerland. This article is an open access article distributed under the terms and conditions of the Creative Commons Attribution (CC BY) license.

1. Introduction

Ordinary Portland cement (OPC) production accounts for 5% to 8% of global CO_2 emissions [1,2], which puts pressure on the construction sector to reduce its environmental impact. In response, geopolymer concrete (GPC) has been identified as a promising eco-friendly alternative. For instance, Smith et al. [3] demonstrated that fly ash-based GPC reduces carbon emissions by up to 56% compared to an equivalent 50 MPa grade conventional OPC concrete. Beyond its environmental benefits, GPC exhibits comparable, and in some cases even superior, mechanical and durability properties to those of OPC concrete [4–6]. In the study of Ramujee et al. [4], three grades of GPC, including 20 MPa, 40 MPa, and 60 MPa, were developed and compared with the equivalent compressive strength of OPC concrete counterparts, and it is reported that the elevated-temperature curing GPC exhibited similar splitting tensile strength when compared to their counterparts. Ambient-cured blended slag/fly ash-based GPC has been shown to gain compressive strength rapidly at early ages and then maintain this strength with time, with a modulus of elasticity of approximately 30 GPa to 34 GPa and Poisson's ratios in the range of 0.15 to 0.18, which are similar to values typically reported for OPC concrete, and they remain stable for up to at least 600 days [5]. From a durability perspective, the blended GPC showed enhanced ageing behaviour and superior resistance to chloride ingress, thereby limiting chloride penetration to the reinforcement and improving its corrosion protection [5]. GPC employs a process known as geopolymerisation, in which readily available aluminosilicate materials are activated by alkaline solutions to form a polymeric binder [7]. Ground granulated blast furnace slag (referred to as slag) and fly ash, which are by-products of steel manufacturing processes and coal-fired power plants, respectively, are commonly utilised as precursors in GPC. By incorporating these waste streams, GPC not only mitigates carbon emissions but also alleviates the environmental burden of landfills.

Traditionally, GPC has relied on a two-part mixing system that requires the addition of strong alkaline liquid activators, such as sodium hydroxide (NaOH), to dissolve and react with aluminosilicate precursor materials. However, this liquid activator restricts the practical scaling of GPC because of its complex handling requirements and safety concerns associated with highly corrosive solutions. Another major limitation is the reliance on elevated-temperature curing to enhance the strength of fly ash-based GPC. For example, Hardjito et al. [8] used NaOH (8 M and 14 M molarity) and sodium silicate (Na_2SiO_3), with silica modulus ratio M_s = 2.0, as the alkaline activators to produce fly ash-based GPC. The authors prepared the alkaline solution activator at least 24 h before mixing the concrete. They reported that raising the curing temperature from 30 °C to 90 °C significantly increased the compressive strength. Similarly, Azevedo et al. [9] cured geopolymer paste at a temperature of 65 °C to 90 °C to achieve compressive strength from 45 MPa to about 90 MPa, respectively.

Because elevated-temperature curing is both energy-intensive and challenging for field cast-in-situ applications, many researchers have increasingly investigated ambient-temperature curing instead. Several studies have reported relatively low-strength ambient-cured GPCs, with 28-day compressive strengths ranging from 29.9 MPa to 39.8 MPa [10–15]. In these studies, slag contents of 10% to 35% or 4% to 7% $Ca(OH)_2$ were used to partially replace fly ash, together with NaOH concentrations of 4 M to 16 M. The sodium silicate-to-sodium hydroxide (SS/SH) ratio varied between 1.0 and 2.5, while the alkaline activator-to-binder (AA/B) ratio ranged from 0.35 to 0.60.

In contrast, several other investigations [5,16–28] achieved higher strength (41 MPa to 104 MPa) by incorporating slag, silica fume, and $Ca(OH)_2$ together with a considerable amount and concentration of alkaline activator to produce ambient-cured GPC. In these studies, fly ash replacement by slag ranged from 10% to 100%, with a notable frequency

above 40%. In some cases, silica fume was also blended with fly ash and slag. The following proportions were observed: the SS/SH ratio was 1.5 to 2.5, the AA/B ratio was from 0.40 to 0.57, and the NaOH concentration was from 8 M to 14 M molarity. More recently, Shamsah et al. [29] developed ambient-cured fly ash/slag-based GPC with compressive strengths exceeding 60 MPa using low-molarity NaOH solutions (2 M to 8 M molarity). These findings clearly demonstrate that high-strength ambient-cured GPC can be successfully produced under appropriately designed mix proportions and activator concentration and dosage. Figure 1 shows the compressive strength of ambient-cured GPC developed in previous studies.

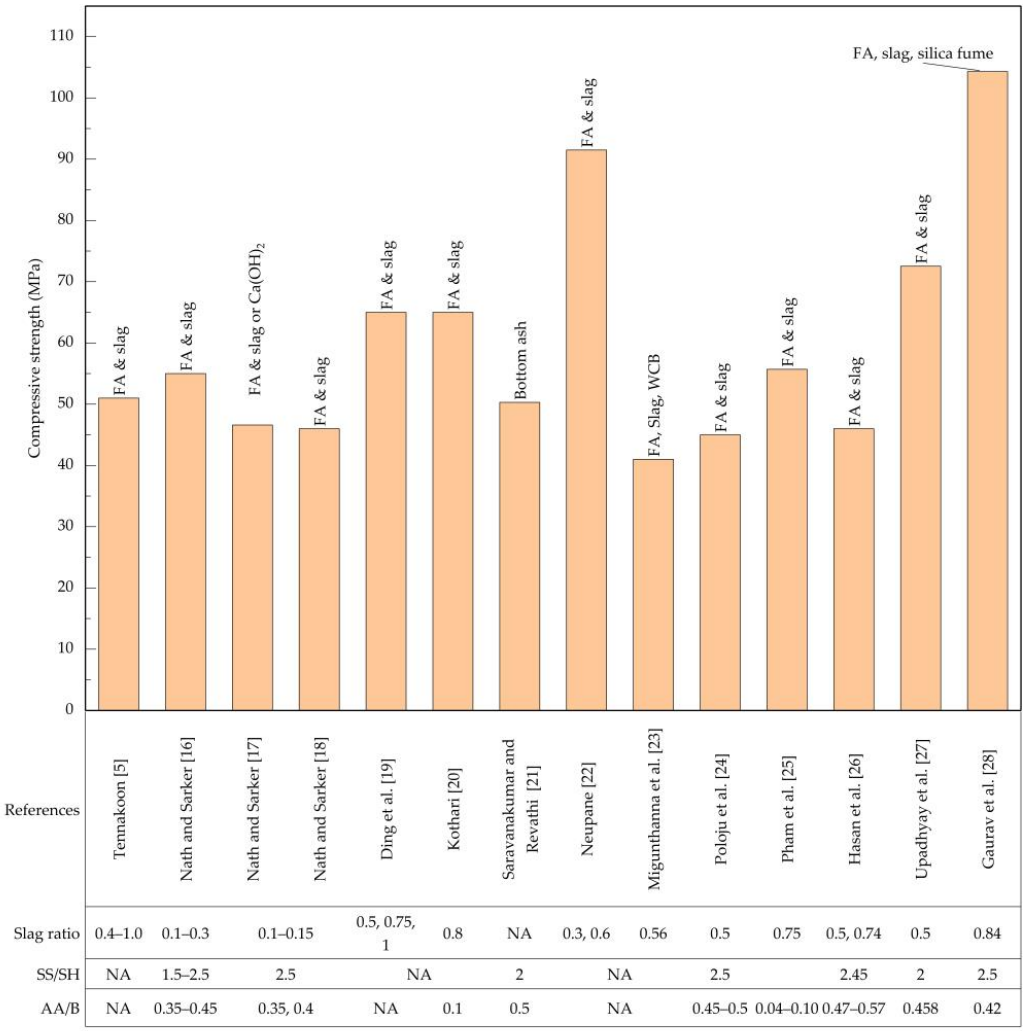


Figure 1. 28-day compressive strength of ambient-cured GPC developed from past studies (source of data: [5,16–28]). Note: SS/SH = sodium metasilicate-to-sodium hydroxide ratio, AA/B = alkaline activator-to-binder ratio, FA = fly ash, and WCB = waste clay brick.

In recent years, attention has shifted toward one-part GPC, which simplifies production through a dry-mix approach, in which aluminosilicate precursors are blended with solid alkaline activators, requiring only the addition of water to initiate the reaction. This is also known as the "just add water" concept, which is the same as the mixing process for OPC concrete. Compared with the traditional two-part system, one-part GPC is safer and easier to handle, transport, and store, making it more suitable for field applications [30]. Despite these advantages, relatively few studies have focused on one-part ambient-cured GPC [5,20,25,31–35]. Most studies primarily focused on compressive strength, splitting tensile strength, and elastic modulus, while limited attention has been given to fracture

energy and uniaxial tensile strength. These latter properties are equally critical for structural design, ensuring the safety of structures during their service lives. Fracture energy governs crack initiation and propagation in concrete structures. Furthermore, to the best of the authors' knowledge, no study has investigated the relationship between splitting tensile strength and uniaxial tensile strength in GPC. While the splitting tensile test is widely used due to its practicality, only uniaxial tensile strength provides the necessary input for structural design, highlighting the need for a correlation between the splitting tensile strength and uniaxial tensile strength.

Unlike most existing studies on one-part ambient-cured GPC that primarily reported compressive strength and general mechanical performance, this study focuses on three underexplored aspects: (i) batch-to-batch reproducibility of mechanical properties under practical production conditions; (ii) fracture-related behaviour through evaluation of fracture energy and uniaxial tensile strength; and (iii) the experimental relationship between splitting tensile strength and direct tensile strength. These contributions provide insight into production reliability and crack and tensile mechanics of one-part ambient-cured GPC, which remain insufficiently documented in the current literature.

2. Experimental Program

The experimental program was structured as a unified investigation in which mix optimisation established a workable and strength-sufficient GPC, mechanical characterisation quantified its structural performance, and reproducibility analysis verified the consistency of these properties under practical production conditions.

2.1. Materials

2.1.1. Precursors and Alkaline Activator

As part of the scope for the main project on the investigation of the performance of fastenings embedded in GPC, this study aimed to produce workable GPC mixes that reached 40 MPa compressive strength at 28 days. Precursor materials were class F fly ash and slag. Slag and fly ash were supplied by Independent Cement & Lime Pty Limited, Port Melbourne, Australia and Cement Australia Pty Limited, Port Melbourne, Australia, respectively. Fly ash had a specific gravity of 2.34, with 98% particles finer than 45 μm. The chemical composition of fly ash was provided by the supplier. For slag, the chemical composition was determined using X-ray fluorescence (XRF) by Juveria et al. [36]. The precursors' chemical properties are given in Table 1. It is worth mentioning that the commercial precursor materials comply with the relevant Australian standards for supplementary cementitious materials (AS 3582.1 [37] for fly ash and AS 3582.2 [38] for slag), supporting the consistency and practical applicability of the materials used in this study. As presented in Table 1, fly ash was primarily composed of 77.5% SiO_2 and 15.3% Al_2O_3, whereas the slag contained 43.82% CaO, 33.03% SiO_2, and 12.42% Al_2O_3. Owing to its low CaO content, fly ash provides an aluminosilicate framework that promotes the formation of N-A-S-H-type gels, while the calcium-rich slag enhances early-age reactivity by supplying readily soluble Ca^{2+} that favours the formation of C–A–S–H gels [39,40].

In this study, granular Na_2SiO_3 (modulus ratio SiO_2/Na_2O = 0.9) supplied by Redox Pty Limited, Laverton North, Australia was used as alkaline activator. SiO_2 content was between 45% and 47%, while the Na_2O proportion was from 49.5% to 51.5%. It was reported that the sole Na_2SiO_3 anhydrous alkaline activator is the most suitable activator when the precursors contain slag and fly ash [32,41]. Figure 2 presents a physical presentation of precursors and the alkaline activator used in this study.

Table 1. Chemical composition of class F fly ash and slag as a percentage of weight.

Oxides	Class F Fly Ash	Slag
SiO_2	77.5	33.03
Al_2O_3	15.3	12.42
CaO	0.3	43.82
Fe_2O_3	3.6	0.38
MgO	0.2	5.57
SO_3	0.1	4.398
K_2O	0.86	0.31
TiO_2	0.5	0.57
P_2O_5	0.2	0.016
MnO	-	0.17
Na_2O	<0.1	0.19
Others	<2	<4
LOI [a]	0.5	0.1

[a] Loss on ignition.



(**a**) (**b**) (**c**)

Figure 2. Binder materials: (**a**) slag, (**b**) fly ash, and (**c**) sodium metasilicate.

2.1.2. Aggregates and Water

This study utilised a combination of medium sand, 14 mm coarse aggregates, and 7 mm screenings. The proportioning strategy was adopted as similar to that used in a previous study [42]. The modification is the replacement of the 10 mm screening adopted in [42] by a 7 mm screening in this current study. The final blend consisted of a sand-to-total-aggregate ratio of 39%, while the 7 mm aggregates constituted 42% of the fraction of total coarse aggregates. The median particle sizes (*D50*) were 0.5 mm, 11.3 mm, and 5.0 mm for the sand, 14 mm, and 7 mm screening, respectively. Figure 3 presents the particle size distribution of coarse aggregates and sand used in this study. The passing percentage graphs were plotted and compared against the Australian Standard for requirements of coarse and fine aggregates intended for use in concrete production, AS 2758.1 [43]. Figure 4 provides a visual representation of the aggregates used. Normal tap water was used for all mixes.

When handling large quantities of aggregates, the process of bringing them to a saturated surface-dry (SSD) condition or drying them is challenging. For large-scale concrete production, using aggregates in their wet or "as-is" condition is, therefore, more practical. In this study, pre-wash wet sand from the supplier was used, and the coarse aggregates were washed and stored in plastic bags or containers. The water absorption and specific gravity of aggregates are tabulated in Table 2. To control the water content of the mixes, the moisture content was determined, and a moisture correction was considered to account for free water in aggregates. An example of moisture correction calculation for determining the as-is weight of aggregates for mixes M12 and M13 (see Table 3) is also provided in Table 2. However, for comparison purposes, and despite practical difficulties, oven-dried aggregates that are commonly used in laboratory settings were also adopted for mixes M13-R3 through M13-R5 in this study, which are presented in Table 4.

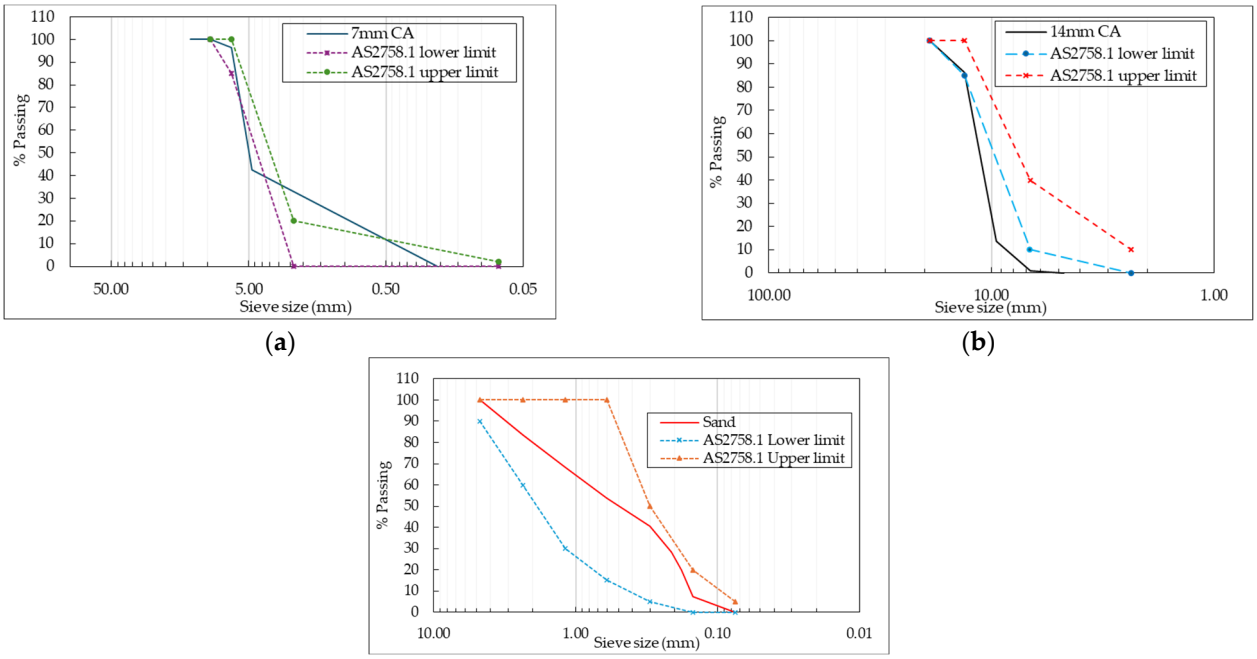


Figure 3. Particle size distribution of: (**a**) 7 mm screening coarse aggregates, (**b**) 14 mm screening coarse aggregates, and (**c**) sand.



Figure 4. (**a**) 14 mm coarse aggregates, (**b**) 7 mm coarse aggregates, and (**c**) sand.

Table 2. Properties of aggregates and moisture correction for M12 and M13.

	Sand	14 mm CA	7 mm CA
WA (%)	0.45	0.55	1.27
Oven-dry weight (kg)	676	619	442
Specific gravity in SSD	2.64	2.69	2.81
SSD weight (kg)	679	622	448
Mc (%)	2.53	0.47	1.36
correction factor	1.021	0.999	1.001
FW (%)	2.08	−0.08	0.09
As-is weight (kg)	693	622	448

Note: FW = free water, WA = water absorption, Mc = moisture content, and SSD = saturated surface dry.

Table 3. Mixture proportions of GPC (kg/m^3).

Mix ID	Nomenclature	Fly Ash	Slag	Na_2SiO_3	Sand	14 mm CA	7 mm CA
M1	FA50SL50-n4.3-W/S40	200	200	34	704	630	456
M2	FA60SL40-n4.3-W/S40	240	160	34	704	630	456
M3	FA50SL50-n4.2-W/S40	200	200	33	704	630	456
M4 [a]	FA50SL50-n4.2-W/S40	200	200	33	766	705	528

Table 3. *Cont.*

Mix ID	Nomenclature	Fly Ash	Slag	Na_2SiO_3	Sand	14 mm CA	7 mm CA
M5	FA50SL50-n4.5-W/S35	200	200	35.7	704	630	456
M6	FA50SL50-n4.8-W/S37	200	200	38	704	630	456
M7	FA60SL40-n5.0-W/S37	240	160	39.6	704	630	456
M8	FA50SL50-n5.0-W/S38	210	210	41.6	704	645	472
M9	FA50Sl50-n5.2-W/S39	220	220	45	703	621	448
M10	FA50Sl50-n5.5-W/S39	220	220	48	703	621	448
M11	FA50Sl50-n5.2-W/S32	220	220	45	708	623	448
M12	FA50SL50-n5.2-W/S38	220	220	45	693	622	448
M13	FA40SL60-n5.2-W/S38	176	264	45	693	622	448

Notes: FA = fly ash, SL = slag, and W/S = water-to-solid ratio. The aggregates were in an as-is condition; therefore, moisture correction and adjustment of external water were considered to fix the W/S ratio. [a] mix M4 is the repeat of mix M3, except for the difference in the aggregate amount.

Table 4. Details of repeated mixes of M13.

Mix ID	Aggregate Conditions and Curing Regimes	Purpose
M13	As-is and moistured curing	Base
M13-R1	As-is and moistured curing	Reproducibility
M13-R2	As-is and moistured curing	Reproducibility and slab casting
M13-R3	Oven-dried and sealed curing	Reproducibility and slab casting
M13-R4	Oven-dried and sealed curing	Reproducibility and uniaxial tensile strength
M13-R5	Oven-dried and sealed curing	Reproducibility and long-term performance

2.2. Mix Proportion

The durability and fresh state behaviour of geopolymer systems are fundamentally governed by pore structure, pore solution chemistry, reaction kinetics, and gel composition [35,44–46]. These microstructures are sensitive to mix design variables such as alkali content, W/S ratio, and slag/fly ash proportions. In this study, the selection of alkali content, W/S ratio, and precursor proportions was contextualised using benchmarks established in the literature to ensure a high-performance matrix that aligns with practical application requirements.

Fresh properties are particularly susceptible to alkali dosage. Studies on binary slag and fly ash-based GPCs show that increasing alkali content from 4% to 6% reduces initial slump and accelerates slump loss over time, reflecting faster reaction kinetics and earlier gel formation [47,48]. When alkali content exceeds about 6% to 7%, mixtures frequently exhibit very low initial slump and rapid loss of flow within a short time after mixing, particularly in slag-rich systems, due to the rapid formation of binding gels [5,46–48]. Tennakoon [5] similarly reports that higher activator contents in ambient-cured GPCs led to faster stiffening and reduced handling time, despite an increase in compressive strength. Overall, alkali dosage directly controls rheological stability and setting time, supporting the choice of 4.2% to 5.5% alkali dosage in the present study to maintain practical fresh behaviour while ensuring sufficient strength development.

The relatively low W/S ratios adopted in this study (0.32 to 0.40) were selected to promote denser matrices and reduced pore connectivity, thereby limiting CO_2 ingress and alkali transport [45,46]. This is consistent with established findings that binary slag and fly ash geopolymer systems with W/S $\leq$ 0.40 exhibit slower carbonation progression than

more porous systems with W/S $\geq$ 0.45 [5,48]. Furthermore, the moderate alkali dosage (about 4% to slightly over 5%) in this study was intended to reduce the likelihood of high concentrations of free mobile alkalis in the pore solution, thereby reducing the potential for efflorescence and carbonation-related issues [35,45]. The balanced fly ash and slag proportions were also selected to promote the formation of a refined gel structure that combines C–(A)–S–H gels and stable N–A–S–H frameworks, contributing to improved microstructural stability [46,48].

In geopolymer binders, drying shrinkage is the macroscopic contraction that occurs as moisture is lost from capillary and gel pores during drying. Drying shrinkage in geopolymer systems is strongly influenced by alkali dosage, W/S ratio, curing regime, and precursor proportions. A recent focused review [49] emphasises that slag-rich binders tend to have finer mesoporous networks (raising capillary stresses), while fly ash-rich binders often exhibit coarser and more permeable porosity (increasing water loss). Consequently, shrinkage is higher than OPC depending on conditions such as curing methods, W/S ratio, and relative humidity [49]. Consistent with this, incorporating fly ash can reduce drying shrinkage compared with slag-based binders [5,49]. Elevated-temperature curing or an ambient-temperature with sealed curing reduced drying shrinkage [49,50]. In addition, higher W/S ratios have been associated with increased drying shrinkage due to coarser and more connected pores [49]. Accordingly, to mitigate shrinkage, this study adopted blended slag and fly ash precursors together with moderate amounts of water and alkaline activator to limit pore connectivity and capillary-driven shrinkage stresses, while maintaining practical fresh state and strength development.

In summary, the mix design parameters in this study are consistent with the literature-reported ranges and were selected to balance between fresh state behaviour, mechanical performance, and long-term durability performance. A detailed mixture proportion is given in Table 3.

Different phases of GPC mixes were carried out to assess workability and compressive strength (see Table 3). Referencing [42], the first group of the mixes (Phase 1, mixes M1 to M4) started with an alkali content (mass of Na_2O/total binders) of 4.3% and 40% to 50% slag (mass ratio to total binders). The definition of mix nomenclature is explained as follows: mixing M1 with FA50SL50-n4.3-W/S40 means that there was 50% fly ash and 50% slag, an alkali content of 4.3%, and a water-to-solid geopolymer ratio of 0.4 or 40%. Keeping alkali content and W/S ratio the same, M2 was the repetition of M1 with a reduction in slag content. M3 and M4 were manufactured to study the effects of alkali content and aggregate content, respectively.

Based on the fresh properties and limited compressive strength observed in Phase 1, Phase 2 mixes (M5 to M8) were developed by increasing alkaline activator dosage, reducing the W/S ratio, and, in some cases, increasing binder content. For example, binder content and alkali content of mix M8 were increased to 420 kg/m^3 and 5%, respectively. Phase 3 mixes (M9 and M10) were developed to improve the compressive strength and workability of Phase 2 mixes. According to the results of Phase 2 mixes, Phase 3 mixes' binder proportion increased to 440 kg/m^3, and the alkali content was 5.2% to 5.5%. On the other hand, Phase 4 mixes, M11 to M13, were made to reduce the W/S of mix M10 and evaluate the suitable proportion of slag. Because the alkaline activator is the most influential driver of cost and CO_2 emission among the mix constituents [51], it is imperative to optimise its dosage in the mix. In this context, Phase 4 mixes M11-M13, with varying fly ash and slag content and different W/S ratios, were limited with a fixed alkali content of 5.2%.

Mix M13 was chosen for detailed evaluation of its mechanical properties because it showed favourable early-age strength and workability with the moderate amount of

alkaline activator used in the mix. Also, after 28 days of curing, M13 would easily pass the target compressive strength required for the large overall project of tensile performance of fastenings in GPC. Table 4 summarises the objectives of these repeated mixes along with the aggregate conditions and curing methods adopted. M13-R1 to M13-R5 were cast to assess the reproducibility of the reference mix (M13). Specifically, M13, M13-R1, and M13-R2 were manufactured using as-is aggregates with moisture curing to represent field-relevant production. In contrast, M13-R3 to M13-R5 were produced using oven-dried aggregates with sealed curing to minimise variability and isolate the effects of aggregate moisture condition and curing regime. In this reproducibility program, the primary focus was to quantify batch-to-batch variation in compressive strength. Therefore, compressive strength was tested across repeat batches, while other mechanical properties were not tested in every batch. In addition to compressive strength evaluation, M13-R4 was assigned to the uniaxial tensile strength test, and M13-R5 was reserved for long-term compressive strength evaluation.

2.3. Mixing and Curing Procedure

2.3.1. Mixing Process

Previous studies reported that the mixing procedure of one-part GPC is the same as that of conventional OPC concrete. For instance, Nematollahi et al. [52] initiated the dry mix of all solid materials, including solid activators, in the Hobart mixer for 2 min for their 3D-printable GPC. Afterwards, tap water was gradually added to the dry mixture, and the mixing process continued for 10 min until a thoroughly mixed mixture was obtained. Similarly, Bong et al. [53] also adopted a similar mixing procedure. Nevertheless, the dry mix of all solid ingredients ended after 3 min. It was reported that the conventional mixing process of OPC concrete was adopted for one-part GPC manufactured in the research studies conducted in Sydney, Australia [54,55]. Collectively, it is confirmed that the mixing procedure for one-part GPC is the same as that typically performed for traditional OPC concrete.

In this study, the mixing time of 15 min was adopted to ensure homogeneous concrete and completely dissolve the granular alkaline activator. The detailed step-by-step mixing procedure is explained in Figures 5 and 6. The sequence of adding water was considered to enhance the workability of GPC. However, to avoid the formation of lumps at relatively low W/S ratios, all the water was added at once for some mixes. For slab casting, a significant amount of material was required. Therefore, it was preferable to extend the mixing time to 20 min to ensure a thorough mix.

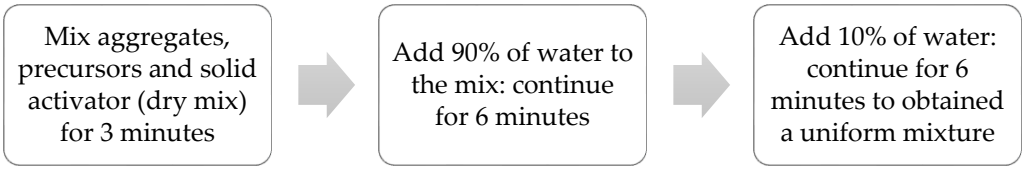


Figure 5. Mixing procedure of one-part GPC.

2.3.2. Curing Method

After casting, all samples were covered with plastic sheets for the first 24 h. After that, the samples were demoulded and cured at ambient temperature (27 ± 3 °C) until the testing dates. To control drying shrinkage while avoiding leaching of the activator because of the curing water, the samples of mixes M1 to M13, M13-R1, and M13-R2 were kept on the spacers and stored in a container. This prevented direct contact between the specimens and curing water. Damp clothes were used to cover the specimens inside the boxes. The

curing process is depicted in Figure 7. For comparison purposes, sealed curing as shown in Figure 8 was adopted for mixes M13-R3 through M13-R5.

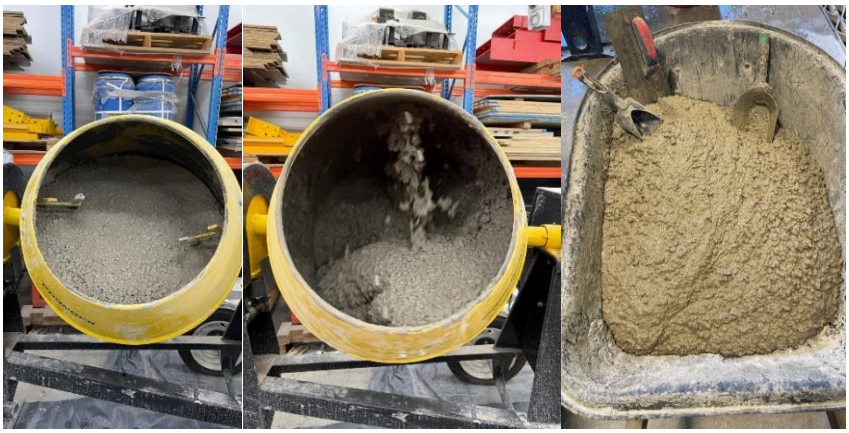
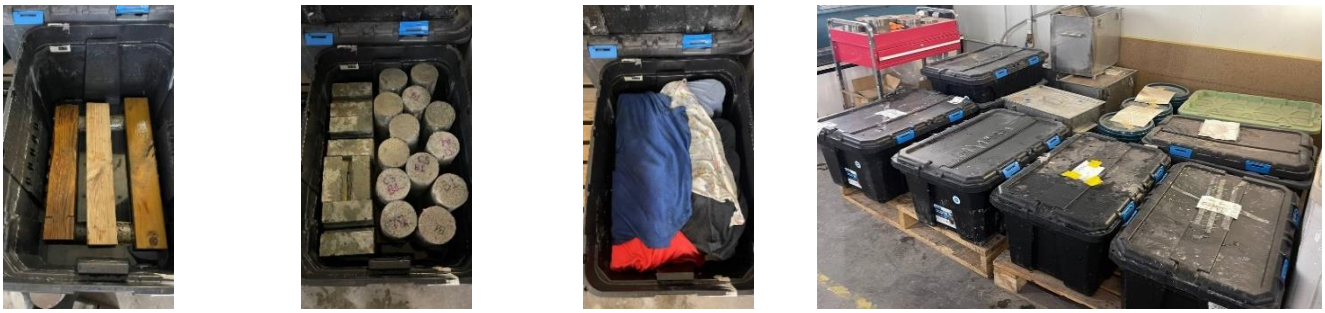


Figure 6. Mixing process and freshly mixed GPC.



(**a**) (**b**) (**c**) (**d**)

Figure 7. Depiction of the curing method (moistured curing): (**a**) Timbers on top of spacers with water underneath, (**b**) placing of specimens over the timbers, (**c**) covering with wet clothes, and (**d**) covering the boxes with the lids.



Figure 8. Sealed curing for mixes M13-R3 through M13-R5.

2.4. Test Methods

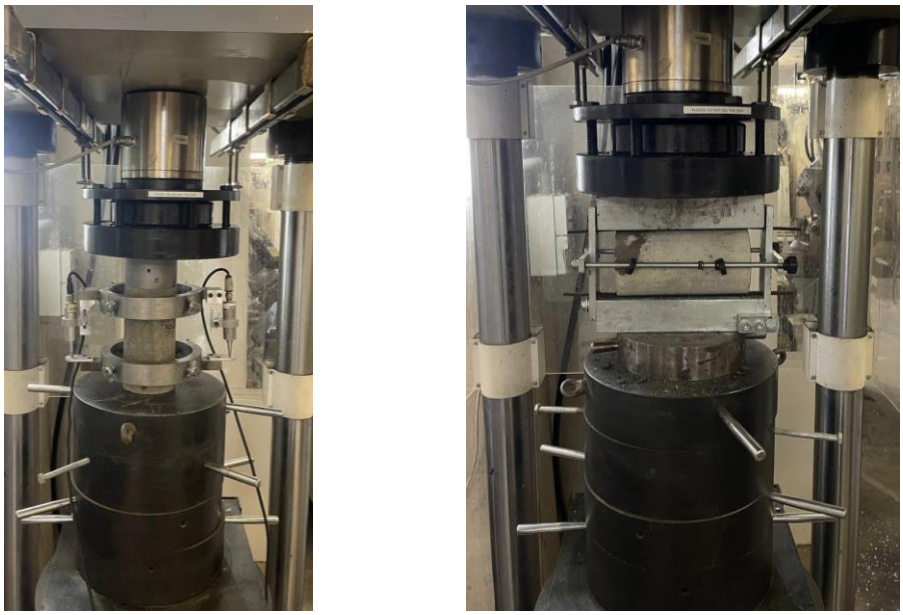
Figure 9 presents the slump test following AS 1012.3.1 [56]. The concrete was placed in the cone in three equal layers, each compacted with 25 strokes. The cone mould was then carefully lifted vertically to allow the concrete to slump. For each batch of mixture, the test was conducted to determine workability and consistency of the fresh GPC.

Table 5 presents the test standards followed in assessing the hardened properties of GPC. Figures 10 and 11 present the physical test setups for modulus of elasticity, splitting

tensile strength, compressive strength, and wedge-splitting tests. Following previous studies [57,58], a load rate of 0.12 mm/min was used for the wedge-splitting test. This small load rate was introduced to ensure that the post-peak behaviour of the specimens was well-captured during the tests. For the wedge-splitting test, a pair of fixtures and a clip gauge were used to measure the displacement of the notches while the vertical load was applied. At the end of the test, the horizontal splitting force and displacement (i.e., crack mouth displacement, CMOD) diagram was obtained. Using the plot obtained, fracture energy was calculated as work energy (i.e., area of the diagram) divided by the ligament area. The detailed geometry of the test specimen can be found in a previous study [58].



Figure 9. Slump measurement of fresh concrete.



(**a**) (**b**)

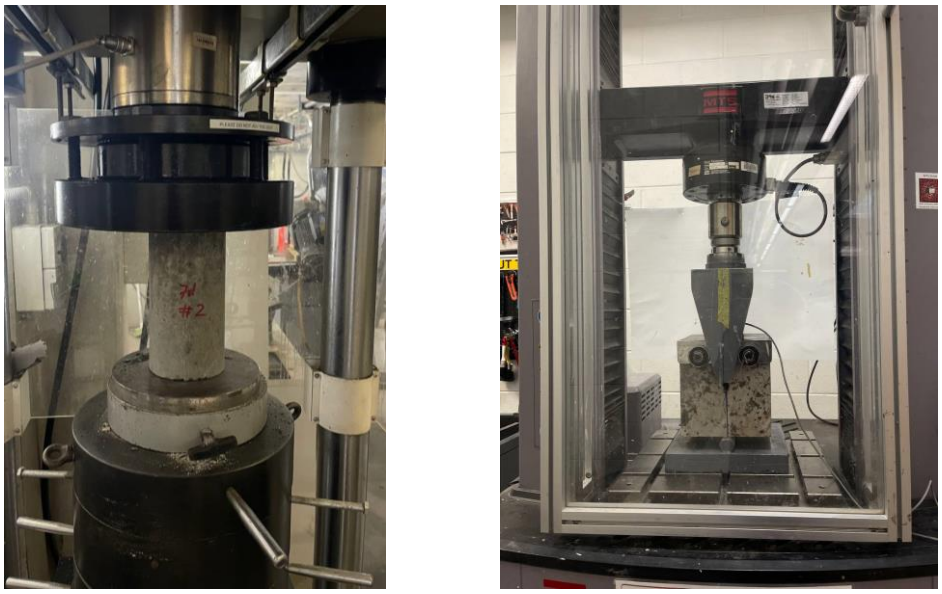
Figure 10. Test setup for: (**a**) modulus of elasticity, and (**b**) splitting tensile strength.

Dog-bone cylindrical specimens were cast and tested until failure to determine the direct tensile strength of GPC. The loading rate was 1 mm/min. The test setup is presented in Figure 12.

Table 5. References used for testing material properties of GPC.

Tests	Dimension of Specimens (mm)	Purpose	Reference
Compressive Strength Test	D100 × 200	Determine the compressive strength of concrete	AS 1012.9 [59]
Modulus of Elasticity	D100 × 200	Determine the modulus of elasticity	AS 1012.17 [60]
Splitting Tensile Strength Test	D100 × 200	Determine indirect tensile strength	AS 1012.10 [61]
Wedge-Splitting Tensile Test	150 × 150 (notched cube)	Determine fracture energy	[62]

Note: D100 × 200 = cylinder that is 100 mm in diameter and 200 mm in height.



(**a**) (**b**)

Figure 11. Test setup for: (**a**) compressive strength, and (**b**) wedge-splitting.



Figure 12. Test setup for uniaxial/direct tensile strength.

3. Results and Discussion

3.1. Fresh Properties

Table 6 summarises the slump measurement, approximate handling time, and initial setting time of the developed GPC. The measured slumps ranged from 20 mm to 230 mm. With the lowest W/S ratio of 0.32, mix M11 achieved only 20 mm slump height, which is not desired for field applications. It is worth mentioning that even after adding small amounts of water to facilitate concrete placement, the mix M11 slump height was still very low, which can be attributed to the flash setting of this specific mix. Previous studies have similarly shown that a lower W/S ratio accelerates setting due to faster geopolymerisation kinetics [63]. In addition, high alkali content (Na_2O) is known to significantly reduce both initial and final setting times, sometimes leading to flash setting in slag-rich geopolymer systems [64]. Choi & Lee [64] reported that slag-based paste with 6% to 8% Na_2O experienced rapid setting when compared to 4% Na_2O.

Table 6. Fresh properties of GPC.

Mix ID	Nomenclature	Slump (mm)	Handling Time (min)	Initial Setting Time (min)
M1	FA50SL50-n4.3-W/S40	120	60	-
M2	FA60SL40-n4.3-W/S40	150	60	-
M3	FA50SL50-n4.2-W/S40	125	60	-
M4	FA50SL50-n4.2-W/S40	55	60	-
M5	FA50SL50-n4.5-W/S35	70	60	-
M6	FA50SL50-n4.8-W/S37	150	60	-
M7	FA60SL40-n5.0-W/S37	60	60	-
M8	FA50SL50-n5.0-W/S38	50	60	-
M9	FA50Sl50-n5.2-W/S39	200	60	-
M10	FA50Sl50-n5.5-W/S39	210	60	-
M11 [a]	FA50Sl50-n5.2-W/S32	20	5	-
M12	FA50SL50-n5.2-W/S38	230	60	-
M13	FA40SL60-n5.2-W/S38	210	60	180

Notes: [a] Mix M11 experienced quick setting, and it was hard to finish the compaction. An additional amount of water (W/S > 0.32) was required to facilitate the concrete placement. Handling time is the estimated period between when the mixing is finished and when the geopolymer concretes (GPCs) begin to harden.

Comparing mixes M1 and M2, it could be concluded that a higher content of fly ash improves the workability of fresh concrete. This observation is in line with previous studies [65–67]. This is due to the smooth spherical shape of the fly ash particles, which is called the ball-bearing effect. A slight difference in alkaline activator dosage had little effect on workability.

Relative to mix M3, increasing the aggregate content in mix M4 remarkably decreased workability. As the aggregate fraction increased, the available paste to effectively bind the particles decreased, which increased the cohesion between the GPC ingredients, hence reducing workability. This finding is consistent with previous studies on both conventional OPC concrete and GPC [68–71]. Consistent with the same mechanism, the slumps of mixes M9, M10, M12, and M13 were significantly higher than those of mixes M1 to M4. This occurred despite slightly lower W/S and nearly identical aggregate content because these mixes contained more binder. For instance, Haruna et al. [33] reported that one-part fly ash-based GPC workability was dependent on the paste-to-aggregate ratio. With the ratio

of 0.35, the slump was 34 mm, while a higher ratio of 0.45 and 0.57 resulted in slumps of 100 mm and 165 mm, respectively.

The setting time measured by the Vicat apparatus is normally used for cement paste with normal consistency. Nevertheless, Migunthanna et al. [72] found that the setting time using the Vicat needle apparatus in accordance with AS/NZS 2350.4 [73] for their geopolymer paste prepared with normal consistency was not reliable to reflect the actual setting time of their GPC when compared with the setting time measured by a penetration resistance test following AS 1012.18 [74]. In their study, geopolymer pastes of normal consistency exhibited an initial setting time of about 1 h, whereas mortar extracted from geopolymer concrete and assessed using penetration resistance exhibited a substantially longer and more representative initial setting time of approximately 4 h to 5 h. This difference was explained by the distinct mixture characteristics of GPC, including higher binder-to-water ratios and the presence of aggregates, which influence moisture distribution, reaction progression, and stiffening response.

Consequently, this study determined the setting time of the selected geopolymer mix using mortar extracted via a 4.75 mm sieve (see Figure 13). Based on the AS/NZS 2350.4 [73] criterion, the initial setting time was defined as the elapsed time from the addition of water to the moment the needle first reached a penetration depth below 39 mm. Following this method, the initial setting time was recorded at 3.0 h. It was observed that the mix became very stiff and challenging to handle even before the 3 h initial setting time. This considerable difference was mainly attributed to the thixotropic nature and viscoelastic stiffening of the geopolymer binder [75,76]. At rest, the GPC underwent rapid structural development, forming a temporary rigid network. However, shear stress induced by the Vicat needle during the penetration can disrupt these temporary thixotropic bonds along its path [77]. As a result, the needle passed easily through the mortar even after the bulk material had lost its macroscopic workability. Therefore, an approximate handling time was established as the primary practical guideline to reflect the material's actual field performance.



Figure 13. Setting time test on extracted geopolymer binder measured using Vicat apparatus.

3.2. Compressive Strength

Figure 14 shows the compressive strength of one-part GPC. In general, mixes with higher slag and/or activator content yielded higher compressive strength at all ages. In particular, mix M1 (50% slag) achieved higher strength than mix M2 (40% slag), with 7-day and 28-day compressive strengths of 24 MPa and 31 MPa for M1, compared with 20.5 MPa and 29 MPa for M2. This finding is in line with the outputs from previous studies indicating that increasing slag content accelerates strength development [47,67,78]. The effect is more pronounced at early ages, when the rapid dissolution of slag provides reactive CaO that promotes the formation of a hybrid C–(N)–A–S–H (calcium (alkali) aluminosilicate hydrate) gel network. In blended slag/fly ash-based systems, these hybrid gels arise because Ca^{2+} released from slag integrates with the dissolved Si^{4+} and Al^{3+} from fly ash, while Na^{+} from the activator balances charge, yielding a structurally cross-linked gel network [79,80]. Conversely, a higher amount of fly ash, resulting in reducing CaO from slag, favours slower N–A–S–H network formation, delaying early strength gain [48,81]. After 28 days, however, the compressive strengths of mixes M1 to M3 were similar, reflecting the progressive reaction of fly ash and the gradual densification of the hybrid gel network. Nevertheless, mix M4, containing the highest aggregate content, exhibited relatively low compressive strength. This is likely due to reduced packing efficiency, which increased entrapped air voids, and to a thinner paste coating around aggregates. The reduced paste thickness weakens the interfacial transition zone (ITZ), promoting stress concentration and decreasing the overall load-bearing capacity.

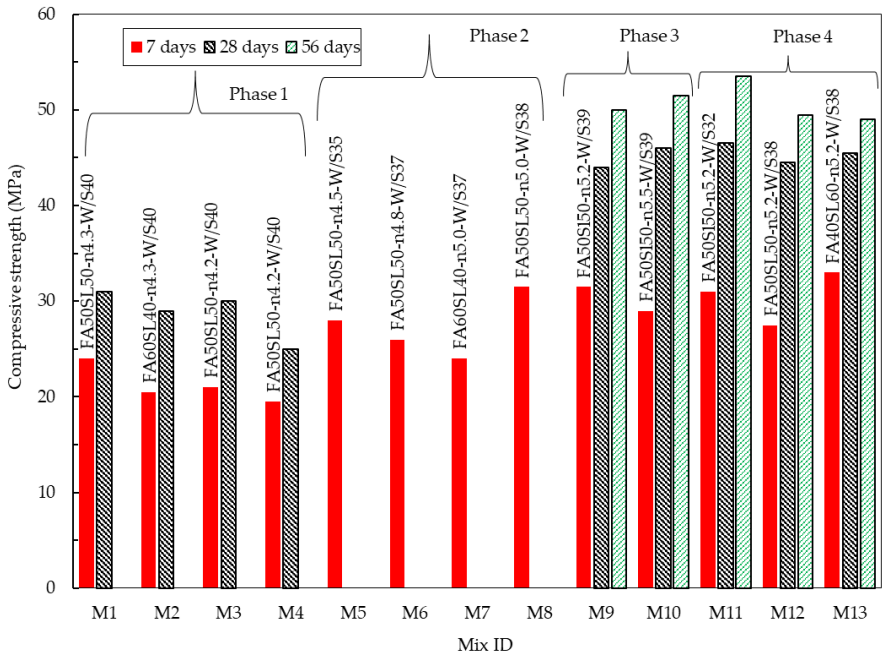


Figure 14. Compressive strength of GPC, mixes M1 to M13, developed at different phases.

Despite adopting the same W/S = 0.4, binder proportions, and alkali content, mix M1 in the present study had lower compressive strength (i.e., 31 MPa after 28 days) than the referenced mixes in the literature; the 28-day compressive strength of the mixes in the literature was between 40 MPa and 45 MPa [42]. This difference is mainly due to the inherent variations in raw materials used in both studies. In particular, the compressive strength of GPC is strongly influenced by the fineness, chemical composition, and amorphous content of the slag and fly ash materials.

As shown in Figure 14, the 7-day compressive strength improved noticeably in Phase 2 (i.e., mixes M5 to M8). This strength enhancement is due to the combined effects of

increased alkali content, a decreased W/S ratio, and higher binder content. These conditions enriched the pH in the environment, which accelerated aluminosilicate dissolution and promoted geopolymer gel formation, resulting in a denser and less porous microstructure in GPC specimens. Despite a remarkable gain in compressive strength in Phase 2, only M6 exhibited acceptable workability, with a slump height of 160 mm. Moreover, based on strength development observed in Phase 1, it was anticipated that only mixes M5 and M8 would reach at least 40 MPa at 28-day age. Although mix M8 exhibited the highest strength, its poor slump reflects limited workability during concrete placement.

By increasing the amount of binder and activator simultaneously, the compressive strength was enhanced. This trend is indicated by comparing the strength of mix M8 against mixes M5 and M6. Accordingly, Phase 3 mixes M9 and M10 were manufactured with a binder content of up to 440 kg/m^3, an alkali content of 5.2% to 5.5%, and a slightly higher W/S ratio than mix M8 in Phase 2. As expected, mixes M9 and M10 exhibited high compressive strength at 28 days, achieving 46 MPa and 46.5 MPa, respectively. The workability was also satisfactory for pouring the concrete slab.

The effect of early-age strength improvement was noticeable with the increase in slag content in the binder. After 7 days of curing, mix M13 showed a compressive strength of 33 MPa, surpassing the 27.5 MPa achieved by mix M12. However, at the ages of 28 and 56 days, the strengths of both mixes were fairly similar. It is worth noting that an additional amount of water (W/S = 0.34, beyond the target W/S of 0.32) was required to ease the concrete placement of mix M11. Hence, the strength level that M11 achieved, presented in Figure 14, corresponds to a W/S of 0.34.

From Phase 3 and 4 mix results, it can be concluded that the 7-day compressive strength attained 62% to 73% of the corresponding 28-day strength, while the 28-day compressive strength reached 87% to 93% of the 56-day strength.

Mix M13 was chosen for the material properties study and full-scale study of fastenings in GPC as part of the entire overall project. Compared to mix M12, mix M13 is more favourable due to its higher early-age compressive strength. In field applications, the speed of construction is a key factor for a cost-effective project; therefore, using high early-age-strength concrete is more desirable.

Long-term strength development of GPC is also presented for mixes M13-R4 and M13-R5, which is illustrated in Figure 15. It is shown that the 90-day strengths were almost the same compared to the 56-day strength. However, there was a slight strength drop for mix M13-R5 after 90 days of curing. A similar trend of strength stability after 56 days of ageing is observed in the previous works on one-part ambient-cured GPC [5,41,55].

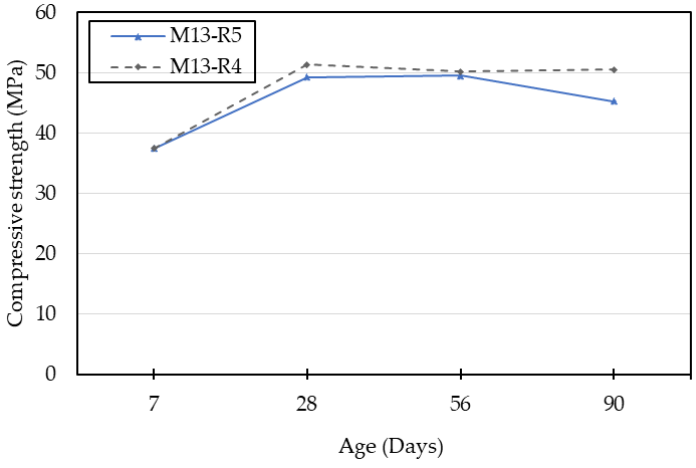


Figure 15. Long-term strength development of GPC mixes M13-R4 and M13-R5.

3.3. Mix Reproducibility, Aggregate Conditions, and Curing Regimes Effect

3.3.1. Compressive Strength of Repeated Mixes

Table 7 presents the compressive strengths of mix M13 and its corresponding repeated mixes. The reported mean strength included the outliers in the dataset. Most mixes had essentially reached their full compressive strength by 28 days, as indicated by 28-day to 56-day strength ratios of 97% to 102%, indicating that the geopolymerisation reactions were substantially complete within the first month of curing. The only exception was mix M13, which achieved only about 88% of its 56-day strength at 28 days, suggesting slower strength development in this batch. Consistent with this behaviour, mix M13 also recorded the lowest compressive strengths at both 7-day and 28-day ages. However, by 56 days, it matched the strengths of the other mixes. It even surpassed M13-R3 by about 5 MPa, confirming that the initial lag in strength gain was temporary and that its long-term performance was ultimately similar to, or exceeded, that of the other mixes. There is no clear indication to explain this initial delay in strength gain. This delay might be attributed to the lower free water content of about 14 kg from aggregates in mix M13 compared against M13-R1 and M13-R2, where free water contents were about 40 kg and 25 kg, respectively. The large additional amount of water in mix M13 may have limited activator mobility and thus delayed initial geopolymerisation. With a significant amount of additional water, the concentration of alkalinity is low at the early stage of curing, resulting in a lesser number of dissolved alkali species moving through the pore solution and reaching the reactive precursor's surfaces.

Table 7. Compressive strength of mix M13 and its repetitions (including outliers).

Aggregate Condition and Curing Regimes	Age (Days)	Mix ID	*n*	f_{cm} (MPa)	STD (MPa)	COV (%)	Strength Gains Relative to 56-Day Strength
As-is aggregates & moistured curing	7	M13	5	31.1	2.82	9.1	64%
As-is aggregates & moistured curing		M13-R1	5	38.3	3.99	10.4	-
As-is aggregates & moistured curing		M13-R2	4	38.8	4.57	11.8	77%
OD aggregates & sealed curing		M13-R3	3	38.5	1.32	3.4	88%
OD aggregates & sealed curing		M13-R4	3	37.5	1.00	2.7	75%
OD aggregates & sealed curing		M13-R5	3	35.5	3.50	9.9	72%
As-is aggregates & moistured curing	28	M13	5	42.8	4.06	9.5	88%
As-is aggregates & moistured curing		M13-R1	5	51.6	0.89	1.7	-
As-is aggregates & moistured curing		M13-R2	3	50.7	1.53	3.0	101%
OD aggregates & sealed curing		M13-R3	8	44.1	1.86	4.2	101%
OD aggregates & sealed curing		M13-R4	3	51.3	2.57	5.0	102%
OD aggregates & sealed curing		M13-R5	3	47.8	0.58	1.2	97%
As-is aggregates & moistured curing	56	M13	5	48.6	0.96	2.0	100%
As-is aggregates & moistured curing		M13-R2	6	50.2	6.49	12.9	100%
OD aggregates & sealed curing		M13-R3	18	43.6	5.60	12.9	100%
OD aggregates & sealed curing		M13-R4	3	50.2	1.89	3.8	100%
OD aggregates & sealed curing		M13-R5	3	49.5	4.09	8.3	100%

Note: OD = oven-dried, *n* = number of cylinders tested, STD = standard deviation, COV = coefficient of variation, and f_{cm} = cylinders' mean compressive strength. There was no test for M13-R1 at 56 days of age. The hardened density was in the range of 2332 kg/m^3 to 2421 kg/m^3.

On both days 28 and 56, the two series of mixes exhibited similar compressive strengths. After 28 days, the values ranged from about 43 MPa to 51 MPa. At 56 days, the as-is aggregates with moisture-curing mixes reached 49 MPa to 50 MPa, and the oven-dried aggregates with sealed curing mixes reached 43 MPa to 50 MPa.

3.3.2. Reproducibility

The coefficients of variation (COV) values of most mixes are approximately 2% to 10%, which fall within the range that is acceptable for laboratory concrete testing. While a few batches in both regimes displayed COV between about the 10% and 13% range, these values are still considered insignificant. In particular, the occurrences were less frequent. They did not correspond to a systematic difference in mean compressive strength between the two curing regimes, reinforcing the conclusion that both the as-is aggregate condition with moisture curing and oven-dried aggregate condition with sealed curing methods had no profound effect on either the level of GPC mean compressive strength or the reproducibility of the GPC.

This small variation is likely linked to the relatively high water content (W/S = 0.38) adopted in this mix, which may create numerous air voids or pores across the cylinder specimens. A similar trend was observed for mix M6, where W/S = 0.37 and COV = 15%, and M10, where W/S = 0.39 and COV = 11.7%. Pore heterogeneity, considering locations, shapes, and sizes, led to premature failure in some specimens under compression. Previous studies reported that the abundant amount of water could impair concrete compressive strength due to the increase in pore volume and/or pore diameter of hardened geopolymer products [82–84]. A higher W/S ratio produced more unreacted particles, whereas a lower ratio yielded a more homogeneous microstructure and a greater formation of gel [84]. Similar findings were indicated by Yang et al. [84], who demonstrated that an increase in liquid-to-solid ratio enlarges porosity and the most probable pore diameter, and, therefore, reduces gel content. Figure 16 illustrates several failed cylinder specimens, revealing variations in pore diameter, location, and shape. Such pores can introduce local weaknesses and contribute to variations in the compressive strength of GPC both within and between the batches. As shown in Figure 16, in some regions of the fractured specimens, dark-coloured areas were observed; these are likely zones of unreacted particles that may further reduce the strength of the cylinders.



Figure 16. Air voids or pores (highlighted in red circles) inside the failed cylinder specimens.

Before the assessment of compressive-strength-related reproducibility of mix M13, formal statistical analysis was carried out to screen the dataset outliers. To ensure scientific rigour, it is advisable for researchers to employ statistical techniques for identifying anomalies. Based on multiple techniques to study treatment approaches for the outliers, Cangussu et al. [85] suggested utilising the Dixon Criteria or the T-statistic as outlined in ASTM E178 [86]. In this study, the Dixon Criteria were employed for the outliers' treatment process. The Dixon Criteria approach is a rank-based statistical procedure for detecting extreme observations in small datasets. ASTM E178 [86] provides the formulation and critical values for this method, allowing objective identification of outliers based on the relative gap between the suspected value and the rest of the data. Firstly, the data must be sorted from smallest to largest value. Then, the following formulas can be used to assess the suspected outliers:

$r_{10} = (x_2 - x_1)/(x_n - x_1)$ when the smallest value is suspected, and the sample size is in the range of 3 to 7.

$r_{22} = (x_3 - x_1)/(x_{n-2} - x_1)$ when the smallest value is suspected, and the sample size is in the range of 14 to 50.

The data is identified as an outlier when the r_{10} or r_{22} is larger than r_{cri}. Table 8 presents the calculated r_{10} and r_{22} together with the critical 5% level of significance. Accordingly, only two values of compressive strength were defined as dataset outliers. It is worth mentioning that only the dataset with a COV higher than 9%, presented in Section 3.3.1, was considered in the outlier screening process. The dataset with a COV less than 9% was considered insignificant and not included in the outlier analysis. As presented in Table 8, only two individual compressive strengths of M13-R2 were detected as outliers.

Table 8. Dataset outlier screening based on Dixon Criteria.

Age	Mix ID	Individual Compressive Strength (MPa)	*n*	Suspected Outliers	r_{10} or r_{22}	r_{cri}	Decision
7	M13	28, 29, 30.5, 33.5, 34.5	5	28	0.154	0.642	Not outlier
	M13-R1	32, 38, 38, 41.5, 42	5	32	0.600	0.642	Not outlier
	M13-R2	32, 40, 41, 42	4	32	0.800	0.766	Outlier
	M13-R5	31, 37, 38	3	31	0.857	0.941	Not outlier
28	M13	37.5, 40, 43.5, 45.5, 47.5	5	37.5	0.250	0.642	Not outlier
56	M13-R2	38, 50, 51, 51, 54, 57	6	38	0.632	0.562	Outlier
56	M13-R3	32.5, 35, 37.5, 39, 40, 40, 40.5, 41, 42, 43, 45, 45, 46, 46.5, 48, 49.5, 50.5, 51, 52	18	32.5	0.278	0.475	Not outlier

After excluding outliers, the 28-day compressive strengths of mixes M13 to M13-R5 fell within a relatively narrow band of 42.8 MPa to 51.6 MPa (range = 8.8 MPa). A similar spread was observed at 56 days, with mean strengths ranging from 43.6 MPa to 52.6 MPa (range = 9.0 MPa). The COV across all datasets ranged from 1.2% to 12.9%, with the majority of results exhibiting COV < 10% (see Table 9), indicating generally good repeatability in compressive strength. Overall, the results do not show a consistent or systematic difference in either the 28-day or 56-day mean compressive strength or COV between mixes produced with as-is aggregates and moisture curing and those produced with oven-dried aggregates and sealed curing. This suggests that, within the investigated parameters, neither aggregate moisture condition nor curing regime significantly affected the reproducibility of compressive strength.

Table 9. Reported compressive strength of all mixes (after filtering out the outliers).

Mix ID	7 Days			28 Days			56 Days		
	f_{cm} (MPa)	STD (MPa)	COV (%)	f_{cm} (MPa)	STD (MPa)	COV (%)	f_{cm} (MPa)	STD (MPa)	COV (%)
M13	31.1	2.82	9.1	42.8	4.06	9.5	48.6	0.96	2
M13-R1	38.3	3.99	10.4	51.6	0.89	1.7	-	-	-
M13-R2	41.0	1.0	2.4	50.7	1.53	3	52.6	2.88	5.5
M13-R3	38.5	1.32	3.4	44.1	1.86	4.2	43.6	5.6	12.9
M13-R4	37.5	1.0	2.7	51.3	2.57	5	50.2	1.89	3.8
M13-R5	35.5	3.5	9.9	47.8	0.58	1.2	49.5	4.09	8.3

Note: STD = standard deviation, COV = coefficient of variation, and f_{cm} = cylinders' mean compressive strength. Strikethrough numbers are considered outliers and thus not included in the mean and COV calculation.

The variability in compressive strength results was assessed using the COV and interpreted in accordance with the quality control classifications provided in ACI 214R-11 [87]. Since the objective of this study is to evaluate batch-to-batch reproducibility of the mix, the variability was assessed using the overall COV as defined in the code. The measured COV values were benchmarked against both laboratory trial batch limits and general construction testing limits outlined in the code. For concretes with strengths exceeding 34.5 MPa, ACI 214R-11 classifies overall variation as excellent when COV < 3.5% for laboratory trial batches and <7% for general construction testing; it is classified as very good at 3.5% to 4.5% (laboratory) and 7% to 9% (general construction); classified as good when COV is 4.5% to 5.5% (laboratory) and 9% to 11% (general construction); and classified as fair when COV is 5.5% to 7% (laboratory) and 11% to 14% (general construction). Most of the results are classified as either excellent or very good control when compared to the benchmarks for the laboratory trial batch. In the general construction category, the results predominantly show excellent control. Only a few batches approach the upper end of the "good" range or fall into the "fair" range. Overall, this ACI-based interpretation confirms that the developed one-part ambient-cured GPC mix exhibits strong batch-to-batch reproducibility.

The scatter plots for mixes M13, M13-R2, and M13-R3 are presented in Figure 17. At 56 days, M13 exhibited the lowest dispersion about the mean, whereas M13-R2 and M13-R3 showed greater scatter.

3.4. Modulus of Elasticity

From Table 10 and Figure 18, it is suggested that the developed GPC reached its full stiffness performance (modulus of elasticity) after 7 days of curing. This finding is in line with a previous study [5]. It has been reported that the modulus of elasticity of blended slag/fly ash-based ambient-cured GPC was between 30 GPa and 34 GPa for 28 days up to 600 days, corresponding to about 45 MPa to 60 MPa compressive strength [5]. It has been demonstrated that the increase in slag content enhanced the modulus of elasticity of GPC [5]. In the present study, the results revealed that the modulus of elasticity of the manufactured GPC ranged from about 30 GPa to 35 GPa. It is observed that, despite lower compressive strength, some batches achieved similar or even slightly higher modulus of elasticity. This behaviour can be linked to variations in precursor composition, which influence gel chemistry, microstructural homogeneity, and porosity. Duxson et al. [88] demonstrated that the modulus of elasticity in geopolymers is governed more by microstructural refinement than by compressive strength alone, where increasing the silica-to-alumina ratio to around 1.65 produced a denser aluminosilicate network and significantly enhanced stiffness. Similarly, Ji et al. [89] reported that increasing alkali content up to an optimal level (8%) accelerates geopolymer gel formation and promotes matrix densification. However, excessive alkali

led to excess gel accumulation, microcracking, and larger pore volumes, which, in turn, reduced mechanical performance. Furthermore, Mohammed et al. [90], in a review of 265 data points from 25 different studies, found only a moderate correlation between compressive strength and modulus of elasticity (R^2 = 0.642), highlighting significant scatter. However, when the authors simultaneously related the modulus of elasticity to concrete density and compressive strength, the correlation was improved (R^2 = 0.857). This finding implies that the modulus of elasticity is more relevant to the densification characteristics of the geopolymer products rather than the compressive strength itself.

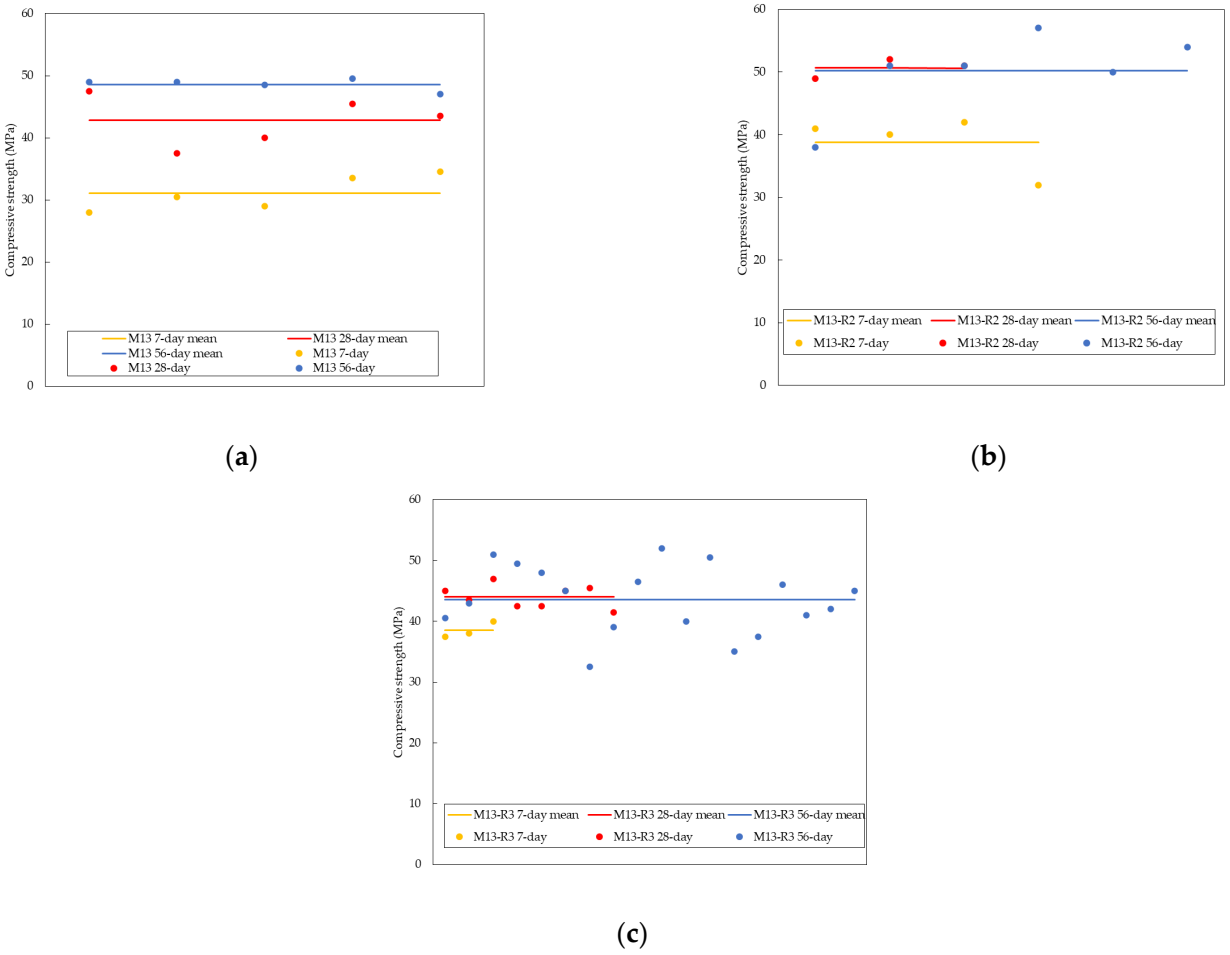


Figure 17. Individual compressive strength of mixes: (**a**) M13; (**b**) M13-R2, as-is aggregates with moisture curing; and (**c**) M13-R3, oven-dried aggregates with sealed curing.

Table 10. Modulus of elasticity of ambient-cured GPC.

Age (Days)	Mix ID	f_{cm} (MPa)	E_C (GPa)	n	COV (%)
7 days	M13-R4	37.5	32.2	2	-
28 days	M13-R3	44.1	32.0	6	8.7
	M13-R4	51.3	30.3	2	-
56 days	M13-R2	52.6	33.7	3	9.7
	M13-R3	48.2	34.8	7	9.9
	M13-R4	50.2	30.7	1	-

Note: n = number of cylinders tested, COV = coefficient of variation, and f_{cm} = cylinders' mean compressive strength.

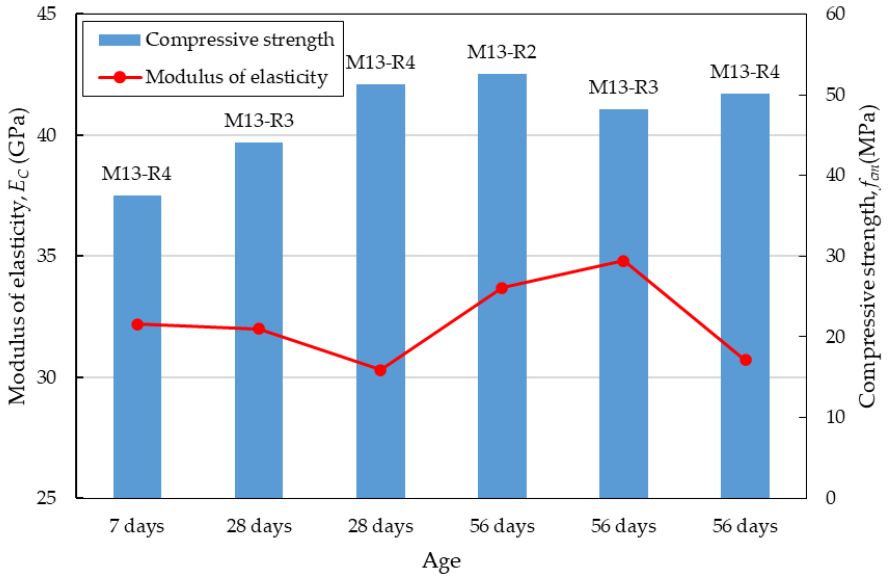


Figure 18. 7-day to 56-day modulus of elasticity of GPC.

The relationship between modulus of elasticity (E_c) and compressive strength of normal OPC concrete based on ACI 318 [91], AS 3600 [92], and Eurocode2 [93] is provided as in Equations (1)–(3), respectively:

$$E_c = 4700\sqrt{f_c'}\ (\text{MPa}) \tag{1}$$

$$E_c = \rho^{1.5} \times 0.043\sqrt{f_{cmi}}\ (\text{MPa})\ \text{if}\ f_{cmi} \leq 40\ \text{MPa; or}$$

$$E_c = \rho^{1.5} \times \left(0.024\sqrt{f_{cmi}} + 0.12\right)\ (\text{MPa})\ \text{if}\ f_{cmi} > 40\ \text{MPa} \tag{2}$$

$$E_c = 22(f_{cm}/10)^{0.3}\ (\text{MPa}) \tag{3}$$

where ρ = density of hardened concrete.

Table 11 lists the prediction equations for determining the modulus of elasticity of ambient-cured GPC suggested in previous studies. Figure 19 shows the comparison of the modulus of elasticity for GPC developed in the current study against existing prediction equations. The modulus of elasticity of the developed GPC closely agreed with the prediction equations for conventional OPC concrete adopted in ACI 318, AS 3600, and Eurocode2. Thus, these equations can be used to determine the modulus of elasticity of blended slag/fly ash-based GPC. Among the equations previously proposed and validated for GPC [14,17,25], only the equation presented by Pham et al. [25], which was validated for GPC with compressive strengths up to 55.7 MPa, demonstrates good agreement with the results of this current study.

Table 11. Correlation between modulus of elasticity and compressive strength for GPC.

Reference Studies	Curing Temperature (°C)	Binders	f_{cm} (MPa)	E_C (GPa)
Lee and Lee [14]	20	FA & slag	15.5–39.1	$E_C = 5.3\sqrt[3]{f_{cm}}$
Nath and Sarker [17]	18–23	FA & slag or $Ca(OH)_2$	33.3–46.6	$E_C = 3.51\sqrt{f_{cm}}$
Pham et al. [25]	ambient	FA & slag	23.6–55.7	$E_C = 5.09\sqrt{f_{cm}}$

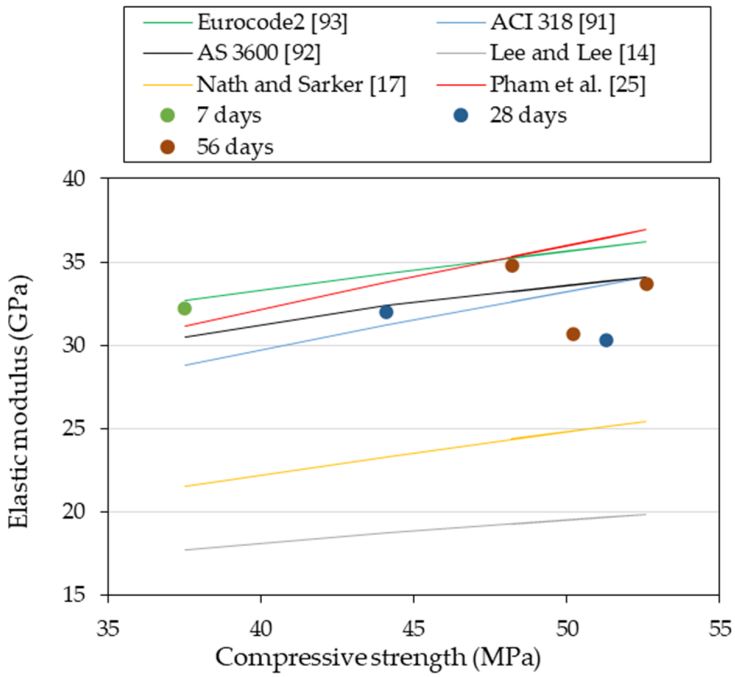


Figure 19. Modulus of elasticity compared to existing prediction equations.

3.5. Splitting Tensile and Uniaxial Tensile Strength

Dog-bone cylindrical specimens were cast and tested for uniaxial tensile strength (f_{ct}). Table 12 presents the splitting tensile and uniaxial tensile strength of GPC. Figure 20 illustrates the typical failure mode of specimens after the end of the splitting tensile strength ($f_{ct.sp}$) test. The ratio between uniaxial tensile strength and splitting tensile strength is equivalent to 0.88, which is comparable to the factor of 0.9 given in the AS 3600 standard [92] for conventional OPC concrete. This indicates that the developed GPC exhibited a similar relationship between uniaxial and splitting tensile strength to that observed in OPC concrete. However, a previous study [94] reported that the splitting tensile strength model based on OPC concrete used in the ACI code [91] and Australian Standard AS 3600 [92] underestimates their GPC's splitting tensile strength. The reported 28-day compressive strength and splitting tensile strength were 49.5 MPa to 59.8 MPa and 2.2 MPa to 4.9 MPa, respectively [94]. The authors reported that compared to similar compressive-strength OPC concrete, the indirect tensile strength is higher than that of the OPC concrete. A similar trend is also observed in the previous studies [89,90].



(**a**) (**b**)

Figure 20. Typical failure mode of splitting tensile strength: (**a**) failure pattern and (**b**) failure surface.

Table 12. Splitting tensile and uniaxial tensile strength of GPC.

Age (Days)	Mix ID	f_{cm} (MPa)	$f_{ct.sp}$ (MPa)	n	COV (%)	f_{ct} (MPa)	n	COV (%)
56	M13-R2	52.6	3.1	3	12.6	-	-	-
	M13-R3	48.2	3.0	8	6.1	-	-	-
	M13-R4	50.2	3.1	4	9.5	2.7	4	10.9

Note: n = number of cylinders tested, COV = coefficient of variation, f_{cm} = cylinders' mean compressive strength, $f_{ct.sp}$ = splitting tensile strength, and f_{ct} = uniaxial tensile strength.

3.6. Fracture Energy

Table 13 reports the fracture energy of GPC developed in this study. Relative to mix M13-R2, the fracture energy of mix M13-R3 had improved by 20%. This improvement may be attributed to the use of a vibrating table to compact mix M13-R3, which potentially reduced entrapped air and enhanced the bonding between the matrix and aggregates. It is worth mentioning that a vibrating table was used to compact mix M13-R3 following the challenges and considerable effort experienced during the manual compaction of mix M13-R2. Despite this change in compaction method, the mean compressive strength of both mixes remained comparable. As presented, the compaction method had a pronounced influence on the fracture energy, but the compressive strength remained relatively stable. This observation is reasonable, as variations in the amount and distribution of entrapped air voids vary the crack propagation behaviour during testing. Consequently, specimens with more uniform compaction exhibited higher fracture energy, since the ultimate load recorded in the wedge-splitting test is highly sensitive to the crack mouth opening displacement and the stability of crack growth.

Table 13. Fracture energy of GPC.

Age (Days)	Mix ID	f_{cm} (MPa)	G_F (N/m)	n	COV (%)
56	M13-R2	52.6	121	6	6.5
	M13-R3	48.2	146	8	11.6

Note: n = number of cylinders tested, COV = coefficient of variation, f_{cm} = cylinders' mean compressive strength, and G_F = fracture energy.

Figures 21 and 22 present the typical failure mode and crack mouth opening displacement (CMOD) diagram of the GPC specimens, respectively.



(**a**) (**b**)

Figure 21. Typical failure mode of wedge-splitting test: (**a**) failure pattern and (**b**) the failure surface.

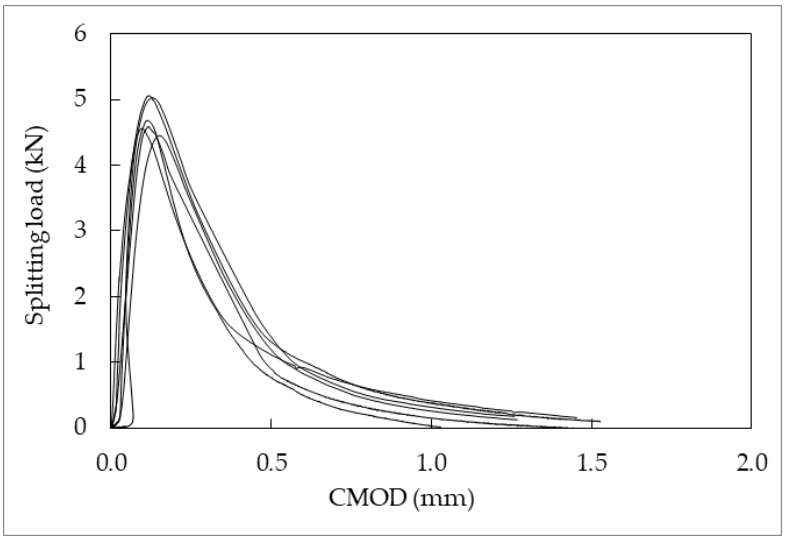


Figure 22. Load and crack mouth opening displacement diagram plotted from wedge-splitting test, M13-R3.

As shown in Table 14, after normalising to a reference compressive strength of 34.5 MPa for comparison purposes, the present mixes (i.e., 79 N/m for M13-R2 and 104 N/m for M13-R3) demonstrate significantly higher fracture energy than the ambient-cured, but they are lower than that of the oven-cured fly ash-based GPC reported in the previous research [95]. This enhancement can be attributed to the blended slag/fly ash binder system used in this study, which accelerated geopolymerisation and yielded a denser matrix. When compared to the existing prediction model for normal OPC concrete, the Fib model code [96] overestimates the actual fracture energy in this current study by 20% for mix M13-R2 and is approximately the same for mix M13-R3. Table 15 shows the comparison of fracture energy in the current study against the existing model.

Table 14. Comparison of fracture energy between this study and previous study.

Study	Mix ID	Binder	f_{cm} (MPa)	G_F (N/m)	$G_{F,adj}$ (N/m)	Remark
This study	M13-R2	Slag and fly ash (one-part)	52.6	121	79	Ambient-cured (manual compaction)
This study	M13-R3	Slag and fly ash (one-part)	48.2	146	104	Ambient-cured (vibrated)
Mohyeddin et al. [95]	Mix 16	Fly Ash only (two-part)	36.6	59.3	55.9	Ambient-cured
Mohyeddin et al. [95]	Mix 10–12	Fly Ash only (two-part)	27.2–37.9	140–153	177–139	Oven-cured at 60 °C for 24 h, and ambient-cured after that
Mohyeddin et al. [95]	OPC	Cement	34.5	142	142	

Note: f_{cm} = cylinders' mean compressive strength, G_F = fracture energy, and $G_{F,adj}$ = adjusted or normalised fracture energy.

Table 15. Comparison of fracture energy against existing prediction models.

Study	Mix ID	f_{cm} (MPa)	G_F (N/m)	Fib Model	G_F/Fib Model	Remark
This study	M13-R2	52.6	121	148.9	0.81	GPC
This study	M13-R3	48.2	146	146.6	0.99	GPC
[95]	OPC	34.5	142	138	1.02	OPC concrete

4. Conclusions

This study advances current knowledge on one-part ambient-cured geopolymer concrete by moving beyond conventional strength reporting to address reproducibility, fracture behaviour, and tensile mechanics. The findings demonstrate the consistency of mechanical performance across repeated batches, provide fracture energy and uniaxial tensile data that are rarely reported for this material, and establish an experimental relationship between splitting tensile and direct tensile strength. These contributions enhance the understanding of the mechanical consistency and crack-related performance of one-part ambient-cured GPC under practical production conditions. The main conclusions drawn from this study are listed as follows:

- Higher slag and activator content both enhanced compressive strength. Higher content of slag increased early-age compressive strength. These findings agree with the results from the literature.
- The compressive strength was improved due to increased alkali content, lower W/S ratio, and increased binder content. However, with the coupling effect of high alkali content and low W/S, GPC experienced fast hardening due to the quick kinetics reaction between alkaline activator and precursors. These effects were in line with previous studies.
- The W/S in GPC must be optimised to balance the trade-off between fresh properties, i.e., workability and setting time, and hardened performance. Excessive water may enhance workability but generally increases porosity, reduces strength, and hardens strength consistency.
- Aggregate conditions and moisture-curing regimes, i.e., as-is aggregates with moisture curing and oven-dried aggregates with sealed curing, had no significant effect on mean compressive strength and reproducibility of GPC. Hence, adopting as-is aggregates using moisture correction to control W/S provides a practical and effective alternative to the conventional oven-dried or saturated surface-dried aggregates method. While the results indicate robust strength reproducibility for the investigated mix, confirmation across a broader range of one-part geopolymer compositions is recommended before extending this conclusion to other geopolymer binders.
- The maximum COV recorded was 12.9%, while most batches showed COV < 10%. This indicates good batch-to-batch reproducibility for mix M13 under both curing regimes, with occasional higher scatter in very few individual batches. When benchmarked against ACI 214R-11 quality control classifications for overall variation, most results fall within the “excellent” (<7%) to “very good/good” (7% to 11%) ranges for general construction testing, while the isolated maximum value remains within the “fair” band (11% to 14%), confirming that the observed variability is generally consistent with acceptable concrete quality control performance.
- The ratio between uniaxial tensile strength and splitting tensile strength for mix M13-R2 was close to 0.9, which is similar to the factor used in the Australian Standard for concrete structures
- The compaction method had a significant effect on the fracture energy of the developed GPC. By adopting the vibrating table, the fracture energy increased by about 17% when compared to manual compaction using the steel rods. The Fib model code is well predicted for the fracture energy of the manufactured specimens adopted with the vibrating table.

Author Contributions: Methodology, D.S.; formal analysis, D.S.; investigation, D.S.; data curation, D.S.; writing—original draft, D.S.; writing—review and editing, J.L., A.M. and J.M.; visualisation, D.S.; supervision, J.L., A.M. and J.M.; project administration, D.S. and J.L.; funding acquisition, J.L. All authors have read and agreed to the published version of the manuscript.

Funding: This research was funded by SmartCrete CRC, grant number P24.172.

Data Availability Statement: The original contributions presented in this study are included in the article. Further inquiries can be directed to the corresponding author.

Acknowledgments: The authors gratefully acknowledge the support of SmartCrete CRC. The authors also extend their sincere thanks to Independent Cement and Lime Pty Ltd. for supplying the commercial slag used in this project. Appreciation is further given to the staff of the Smart Structures Laboratory at Swinburne University of Technology for their ongoing support throughout the research. The authors also wish to acknowledge the contributions of undergraduate final-year research project students for their assistance with concrete ingredient preparation, casting, and materials testing. The authors would like to acknowledge a Master's degree student who contributed to the uniaxial tensile test with the mould preparation and testing works.

Conflicts of Interest: The authors declare no conflicts of interest.

References

1. Niu, L.; Wu, S.; Andrew, R.M.; Shao, Z.; Wang, J.; Xi, F. Global and National CO_2 Uptake by Cement Carbonation from 1928 to 2024. *Earth Syst. Sci. Data* **2025**, *17*, 2231–2247. [CrossRef]
2. Shobeiri, V.; Bennett, B.; Xie, T.; Visintin, P. A Comprehensive Assessment of the Global Warming Potential of Geopolymer Concrete. *J. Clean. Prod.* **2021**, *297*, 126669. [CrossRef]
3. Setiawan, A.A.; Hardjasaputra, H.; Soegiarso, R. Embodied Carbon Dioxide of Fly Ash Based Geopolymer Concrete. *IOP Conf. Ser. Earth Environ. Sci.* **2023**, *1195*, 012031. [CrossRef]
4. Ramujee, K.; Potharaju, M. Mechanical Properties of Geopolymer Concrete Composites. *Mater. Today Proc.* **2017**, *4*, 2937–2945. [CrossRef]
5. Tennakoon, C.K. Assessment of Properties of Ambient Cured Geopolymer Concrete for Construction Applications. Doctoral Dissertation, Swinburne University of Technology, Melbourne, Australia, 2016.
6. Bellum, R.R.; Muniraj, K.; Madduru, S.R.C. Influence of Slag on Mechanical and Durability Properties of Fly Ash-Based Geopolymer Concrete. *J. Korean Ceram. Soc.* **2020**, *57*, 530–545. [CrossRef]
7. Davidovits, J. Properties of Geopolymer Cements. In Proceedings of the First International Conference on Alkaline Cements and Concretes, Kiev, Ukraine, 11–14 October 1994; Kiev State Technical University: Kyiv, Ukraine, 1994; pp. 131–149.
8. Hardjito, D.; Wallah, S.E.; Sumajouw, D.M.J.; Rangan, B.V. On the Development of Fly Ash-Based Geopolymer Concrete. *ACI Mater. J.* **2004**, *101*, 467–472. [CrossRef]
9. Azevedo, A.G.S.; Strecker, K.; Barros, L.A.; Tonholo, L.F.; Lombardi, C.T. Effect of Curing Temperature, Activator Solution Composition and Particle Size in Brazilian Fly-Ash Based Geopolymer Production. *Mater. Res.* **2019**, *22*, e20180842. [CrossRef]
10. Yombi Anne, M.; Chand, J. Geo-Polymer Concrete—A Concrete for Sustainable Environment. *IOP Conf. Ser. Earth Environ. Sci.* **2023**, *1110*, 012049. [CrossRef]
11. Nath, P.; Sarker, P.K. Fracture Properties of Geopolymer Concrete Cured in Ambient Temperature. *SSb* **2013**, *114*, 1061–1066. [CrossRef]
12. Mahmood, A.H.; Foster, S.J.; Castel, A. Development of High-Density Geopolymer Concrete with Steel Furnace Slag Aggregate for Coastal Protection Structures. *Constr. Build. Mater.* **2020**, *248*, 118681. [CrossRef]
13. Adam, A.A. The Effects of Water to Solid Ratio, Activator to Binder Ratio, and Lime Proportion on the Compressive Strength of Ambient-Cured Geopolymer Concrete. *J. Civ. Eng. Forum* **2019**, *5*, 161–168. [CrossRef]
14. Lee, N.K.; Lee, H.K. Setting and Mechanical Properties of Alkali-Activated Fly Ash/Slag Concrete Manufactured at Room Temperature. *Constr. Build. Mater.* **2013**, *47*, 1201–1209. [CrossRef]
15. Venkateswararao, J.; Srinivasa Rao, K.; Rambabu, K.; Brahma Reddy, T. Comparative Study on Mechanical Properties of Geopolymers and Their Composites. *ARPN J. Eng. Appl. Sci.* **2013**, *8*, 10.
16. Nath, P.; Sarker, P.K. Effect of GGBFS on Setting, Workability and Early Strength Properties of Fly Ash Geopolymer Concrete Cured in Ambient Condition. *Constr. Build. Mater.* **2014**, *66*, 163–171. [CrossRef]

17. Nath, P.; Sarker, P.K. Flexural Strength and Elastic Modulus of Ambient-Cured Blended Low-Calcium Fly Ash Geopolymer Concrete. *Constr. Build. Mater.* **2017**, *130*, 22–31. [CrossRef]
18. Nath, P.; Sarker, P.K. Fracture Properties of GGBFS-Blended Fly Ash Geopolymer Concrete Cured in Ambient Temperature. *Mater. Struct. Mater. Constr.* **2017**, *50*, 32. [CrossRef]
19. Ding, Y.; Shi, C.J.; Li, N. Fracture Properties of Slag/Fly Ash-Based Geopolymer Concrete Cured in Ambient Temperature. *Constr. Build. Mater.* **2018**, *190*, 787–795. [CrossRef]
20. Kothari, A. Effects of Fly Ash on the Properties of Alkali Activated Slag Concrete. Master's Thesis, Luleå University of Technology, Luleå, Sweden, 2017.
21. Saravanakumar, R.; Revathi, V. Some Durability Aspects of Ambient Cured Bottom Ash Geopolymer Concrete. *Arch. Civ. Eng.* **2017**, *63*, 99–114. [CrossRef]
22. Neupane, K. High-Strength Geopolymer Concrete- Properties, Advantages and Challenges. *Adv. Mater.* **2018**, *7*, 15. [CrossRef]
23. Migunthanna, J.; Rajeev, P.; Sanjayan, J. Waste Clay Brick Binders for Rigid Pavement Subbase and Base Concretes. In *Lecture Notes in Civil Engineering*; Springer: Cham, Switzerland, 2022; Volume 193, pp. 903–917.
24. Poloju, K.K.; Annadurai, S.; Manchiryal, R.K.; Goriparthi, M.R.; Baskar, P.; Prabakaran, M.; Kim, J. Analysis of Rheological Characteristic Studies of Fly-Ash-Based Geopolymer Concrete. *Buildings* **2023**, *13*, 811. [CrossRef]
25. Pham, T.T.; Nguyen, N.L.; Nguyen, T.T.; Nguyen, T.T.; Pham, T.H. Effects of Superplasticizer and Water–Binder Ratio on Mechanical Properties of One-Part Alkali-Activated Geopolymer Concrete. *Buildings* **2023**, *13*, 1835. [CrossRef]
26. Hasan, M.A.; Sheehan, T.; Ashour, A.; Elkezza, O. Flexural Behaviour of Geopolymer Concrete T-Beams Reinforced with GFRP Bars. *Structures* **2023**, *49*, 345–364. [CrossRef]
27. Upadhyay, D.; Chanda, A.; Thakkar, S. Mixture Design of High-Strength Geopolymer Concrete. *Mater. Today Proc.* **2023**, *93*, 335–339. [CrossRef]
28. Gaurav, J.; Modhera, C.; Patel, D. Proposed Mixture Design Method for High-Strength Geopolymer Concrete. *ACI Mater. J.* **2024**, *121*, 67–78. [CrossRef]
29. Shamsah, M.; Kalfat, R.; Subramaniam, K.V.L. Impact of Low NaOH Molarities on Mechanical and Durability Properties of Ambient and Oven-Cured Fly Ash Geopolymer Concrete. *J. Build. Eng.* **2025**, *105*, 112491. [CrossRef]
30. Stellamary, F.; Madhavi, T.C. Investigations on Ambient Cured Alkali-Activated One-Part Geopolymer Concrete. In *Proceedings of the Emerging Trends in Composite Structures*; Mannan, M.A., Sathyanathan, R., Umamaheswari, N., Chore, H.S., Eds.; Springer Nature: Singapore, 2024; pp. 595–602.
31. Migunthanna, J.; Rajeev, P.; Sanjayan, J. Waste Clay Bricks as a Geopolymer Binder for Pavement Construction. *Sustainability* **2022**, *14*, 6456. [CrossRef]
32. Nematollahi, B.; Sanjayan, J.; Shaikh, F.U.A. Synthesis of Heat and Ambient Cured One-Part Geopolymer Mixes with Different Grades of Sodium Silicate. *Ceram. Int.* **2015**, *41*, 5696–5704. [CrossRef]
33. Haruna, S.; Mohammed, B.S.; Wahab, M.M.A.; Liew, M.S. Effect of Paste Aggregate Ratio and Curing Methods on the Performance of One-Part Alkali-Activated Concrete. *Constr. Build. Mater.* **2020**, *261*, 120024. [CrossRef]
34. Neupane, K. Evaluation of Environmental Sustainability of One-Part Geopolymer Binder Concrete. *Clean. Mater.* **2022**, *6*, 100138. [CrossRef]
35. Luukkonen, T.; Abdollahnejad, Z.; Yliniemi, J.; Kinnunen, P.; Illikainen, M. One-Part Alkali-Activated Materials: A Review. *Cem. Concr. Res.* **2018**, *103*, 21–34. [CrossRef]
36. Juveria, F.; Migunthanna, J.; Rajeev, P.; Sanjayan, J. Mechanical and Fatigue Performance of Recycled Concrete Aggregate Blended with Waste Tyre Rubber Stabilised with Slag for Pavement Application. *Buildings* **2025**, *15*, 3852. [CrossRef]
37. *AS 3582.1*; Supplementary Cementitious Materials for Use with Portland and Blended Cement, Part 1: Fly Ash. Standards Australia: Sydney, Australia, 2016.
38. *AS 3582.2*; Supplementary Cementitious Materials, Part 2: Slag—Ground Granulated Blast-Furnace Slag. Standards Australia: Sydney, Australia, 2016.
39. Ghafoor, M.T.; Rakhimova, N.; Shi, C. One Part Geopolymers: A Comprehensive Review of Advances and Key Challenges. *J. Build. Eng.* **2025**, *111*, 113112. [CrossRef]
40. Mohammed, T.O.; Ul Haq, A.; Harun, M.Z.B.; Fanijo, E.O. Recent Advances in Fly Ash- and Slag-Based Geopolymer Cements. *Sustainability* **2025**, *17*, 11167. [CrossRef]
41. Negahban, E.; Bagheri, A.; Sanjayan, J. Investigation of Abrasion Resistance of Geopolymer Concrete Cured in Ambient Temperature for Pavement Applications. *Road Mater. Pavement Des.* **2023**, *24*, 2641–2662. [CrossRef]
42. Shayan, A.; Tennakoon, C.; Xu, A. *Specification and Use of Geopolymer Concrete in the Manufacture of Structural and Non-Structural Components: Experimental Work*; The National Academies of Sciences, Engineering, and Medicine: Washington, DC, USA, 2017.
43. *AS 2758.1:2014*; Aggregates and Rock for Engineering Purposes, Part 1: Concrete Aggregates. Standards Australia: Sydney, Australia, 2014.

44. Ye, G.; Dehn, F. *Mechanical Properties of Alkali-Activated Materials*; RILEM State-of-the-Art Reports; Springer Nature: Cham, Switzerland, 2026; Volume 46.
45. Lamaa, G.; Duarte, A.P.C.; Silva, R.V.; de Brito, J. Carbonation of Alkali-Activated Materials: A Review. *Materials* **2023**, *16*, 3086. [CrossRef]
46. Bernal, S.A.; Provis, J.L.; Walkley, B.; San Nicolas, R.; Gehman, J.D.; Brice, D.G.; Kilcullen, A.R.; Duxson, P.; Van Deventer, J.S.J. Gel Nanostructure in Alkali-Activated Binders Based on Slag and Fly Ash, and Effects of Accelerated Carbonation. *Cem. Concr. Res.* **2013**, *53*, 127–144. [CrossRef]
47. Deb, P.S.; Nath, P.; Sarker, P.K. The Effects of Ground Granulated Blast-Furnace Slag Blending with Fly Ash and Activator Content on the Workability and Strength Properties of Geopolymer Concrete Cured at Ambient Temperature. *Mater. Des. (1980–2015)* **2014**, *62*, 32–39. [CrossRef]
48. Humad, A.M.; Kothari, A.; Provis, J.L.; Cwirzen, A. The Effect of Blast Furnace Slag/Fly Ash Ratio on Setting, Strength, and Shrinkage of Alkali-Activated Pastes and Concretes. *Front. Mater.* **2019**, *6*, 9. [CrossRef]
49. Mohamed, O.A.; Zuaiter, H.A.; Najm, O. Shrinkage Characteristics of Sustainable Mortar and Concrete with Alkali-Activated Slag and Fly Ash Binders: A Focused Review. *Mater. Today Proc.* 2024; *in press*. [CrossRef]
50. Migunthanna, J.; Rajeev, P.; Sanjayan, J. Shrinkage Model for Waste Clay Brick-Based Geopolymer Concrete. *Constr. Build. Mater.* **2023**, *404*, 133196. [CrossRef]
51. Migunthanna, J.; Rajeev, P.; Sanjayan, J. Investigation of Waste Clay Brick as Partial Replacement of Geopolymer Binders for Rigid Pavement Application. *Constr. Build. Mater.* **2021**, *305*, 124787. [CrossRef]
52. Nematollahi, B.; Bong, S.H.; Xia, M.; Sanjayan, J. Digital Fabrication of 'Just-Add-Water' Geopolymers: Effects of Curing Condition and Print-Time Interval. In *Second RILEM International Conference on Concrete and Digital Fabrication*; RILEM Bookseries; Springer: Cham, Switzerland, 2020; Volume 28.
53. Bong, S.H.; Nematollahi, B.; Xia, M.; Nazari, A.; Sanjayan, J. Properties of One-Part Geopolymer Incorporating Wollastonite as Partial Replacement of Geopolymer Precursor or Sand. *Mater. Lett.* **2020**, *263*, 127236. [CrossRef]
54. Neupane, K.; Kidd, P.; Chalmers, D.; Baweja, D.; Shrestha, R. Investigation on Compressive Strength Development and Drying Shrinkage of Ambient Cured Powder-Activated Geopolymer Concretes. *Aust. J. Civ. Eng.* **2016**, *14*, 72–83. [CrossRef]
55. Neupane, K.; Hadigheh, S.A. Sodium Hydroxide-Free Geopolymer Binder for Prestressed Concrete Applications. *Constr. Build. Mater.* **2021**, *293*, 123397. [CrossRef]
56. *AS 1012.3.1:2014*; Methods of Testing Concrete–Determination of Properties Related to the Consistency of Concrete–Slump Test. Standard Australia: Sydney, Australia, 2014.
57. Al-Yousuf, A.A.Y. Performance of Cast-in Anchors in Early Age Concrete with Supplementary Cementitious Materials (SCMs). Doctoral Dissertation, Swinburne University of Technology, Melbourne, Australia, 2019. [CrossRef]
58. Obayes, O.R. Tensile Behaviour of Post-Installed and Cast-In Mechanical Anchors in Early Age Concrete. Doctoral Dissertation, Swinburne University of Technology, Melbourne, Australia, 2022. [CrossRef]
59. *AS 1012.9*; Methods of Testing Concrete–Compressive Strength Tests–Concrete, Mortar and Grout Specimens. Standards Australia: Sydney, Australia, 2014.
60. *AS 1012.17*; Methods of Testing Concrete. Method 17: Determination of the Static Chord Modulus of Elasticity and Poisson's Ratio of Concrete Specimens. Standards Australia: Sydney, Australia, 1997.
61. *AS 1012.10*; Methods of Testing Concrete–Determination of Indirect Tensile Strength of Concrete Cylinders (Brasil or Splitting Test). Standards Australia: Sydney, Australia, 2000.
62. Brühwiler, E.; Wittmann, F.H. The Wedge Splitting Test, a New Method of Performing Stable Fracture Mechanics Tests. *Eng. Fract. Mech.* **1990**, *35*, 117–125. [CrossRef]
63. Quiatchon, P.R.J.; Dollente, I.J.R.; Abulencia, A.B.; De Guzman Libre, R.G.; Villoria, M.B.D.; Guades, E.J.; Promentilla, M.A.B.; Ongpeng, J.M.C. Investigation on the Compressive Strength and Time of Setting of Low-Calcium Fly Ash Geopolymer Paste Using Response Surface Methodology. *Polymers* **2021**, *13*, 3461. [CrossRef]
64. Choi, S.; Lee, K.M. Influence of Na_2O Content and Ms (SiO_2/NamO) of Alkaline Activator on Workability and Setting of Alkali-Activated Slag Paste. *Materials* **2019**, *12*, 2072. [CrossRef] [PubMed]
65. De Hita, M.J.; Criado, M. Influence of the Fly Ash Content on the Fresh and Hardened Properties of Alkali-Activated Slag Pastes with Admixtures. *Materials* **2022**, *15*, 992. [CrossRef]
66. Laskar, S.M.; Talukdar, S. Preparation and Tests for Workability, Compressive and Bond Strength of Ultra-Fine Slag Based Geopolymer as Concrete Repairing Agent. *Constr. Build. Mater.* **2017**, *154*, 176–190. [CrossRef]
67. Xie, J.; Wang, J.; Rao, R.; Wang, C.; Fang, C. Effects of Combined Usage of GGBS and Fly Ash on Workability and Mechanical Properties of Alkali Activated Geopolymer Concrete with Recycled Aggregate. *Compos. B Eng.* **2019**, *164*, 179–190. [CrossRef]
68. Xu, G.; Wu, H.; Cai, J.; Guo, S.; Zhang, Z.; Shen, W.; Tian, Q. Influence of Mortar Thickness on the Dynamic Segregation of High-Fluidity Concrete. *Constr. Build. Mater.* **2024**, *438*, 137153. [CrossRef]

69. Hu, J.; Wang, K. Effect of Coarse Aggregate Characteristics on Concrete Rheology. *Constr. Build. Mater.* **2011**, *25*, 1196–1204. [CrossRef]
70. Ivanova, I.; Mechtcherine, V. Effects of Volume Fraction and Surface Area of Aggregates on the Static Yield Stress and Structural Build-up of Fresh Concrete. *Materials* **2020**, *13*, 1551. [CrossRef] [PubMed]
71. Vinai, R.; Rafeet, A.; Soutsos, M.; Sha, W. The Role of Water Content and Paste Proportion on Physico-Mechanical Properties of Alkali Activated Fly Ash–Ggbs Concrete. *J. Sustain. Metall.* **2016**, *2*, 51–61. [CrossRef]
72. Migunthanna, J.; Rajeev, P.; Sanjayan, J. Waste Clay Brick as a Part Binder for Pavement Grade Geopolymer Concrete. *Int. J. Pavement Res. Technol.* **2023**, *17*, 1450–1467. [CrossRef]
73. *AS/NZS 2350.4*; Methods of Testing Portland, Blended and Masonry Cements, Method 4: Setting Time. Standards Australia: Sydney, Australia; Standards New Zealand: Wellington, New Zealand, 2006.
74. *AS 1012.18*; Methods of Testing Concrete, Method 18: Determination of Setting Time of Fresh Concrete, Mortar and Grout by Penetration Resistance. Standards Australia: Sydney, Australia, 1996.
75. Mahmoodi, O.; Siad, H.; Lachemi, M.; Dadsetan, S.; Şahmaran, M. Extensive Rheological Evaluation of Geopolymer Mortars Incorporating Maximum Amounts of Recycled Concrete as Precursors and Aggregates. *Constr. Build. Mater.* **2023**, *390*, 131801. [CrossRef]
76. Brandvold, A.S.; Al-Chaar, G.K.; Kriven, W.M. Isolating the Effects of Thixotropy in Geopolymer Pastes. *J. Am. Ceram. Soc.* **2023**, *106*, 2797–2807. [CrossRef]
77. Favier, A.; Habert, G.; D'Espinose De Lacaillerie, J.B.; Roussel, N. Mechanical Properties and Compositional Heterogeneities of Fresh Geopolymer Pastes. *Cem. Concr. Res.* **2013**, *48*, 9–16. [CrossRef]
78. Bernal, S.A.; Provis, J.L.; Rose, V.; Mejía De Gutierrez, R. Evolution of Binder Structure in Sodium Silicate-Activated Slag-Metakaolin Blends. *Cem. Concr. Compos.* **2011**, *33*, 46–54. [CrossRef]
79. Ismail, I.; Bernal, S.A.; Provis, J.L.; San Nicolas, R.; Hamdan, S.; Van Deventer, J.S.J. Modification of Phase Evolution in Alkali-Activated Blast Furnace Slag by the Incorporation of Fly Ash. *Cem. Concr. Compos.* **2014**, *45*, 125–135. [CrossRef]
80. Das, D.; Rout, P.K. Synthesis and Characterization of Fly Ash and GBFS Based Geopolymer Material. *Biointerface Res. Appl. Chem.* **2021**, *11*, 14506–14519. [CrossRef]
81. Bakharev, T. Geopolymeric Materials Prepared Using Class F Fly Ash and Elevated Temperature Curing. *Cem. Concr. Res.* **2005**, *35*, 1224–1232. [CrossRef]
82. Wang, S.-D.; Scrivener, K.L.; Pratt, P.L. Factors Affecting the Strength of Alkali-Activated Slag. *Cem. Concr. Res.* **1994**, *24*, 1033–1043. [CrossRef]
83. Oderji, S.Y.; Chen, B.; Shakya, C.; Ahmad, M.R.; Shah, S.F.A. Influence of Superplasticizers and Retarders on the Workability and Strength of One-Part Alkali-Activated Fly Ash/Slag Binders Cured at Room Temperature. *Constr. Build. Mater.* **2019**, *229*, 116891. [CrossRef]
84. Yang, Y.; Wang, B.; Yuan, Q.; Huang, D.; Peng, H. Characterization, Factors, and Fractal Dimension of Pore Structure of Fly Ash-Based Geopolymers. *J. Mater. Res. Technol.* **2023**, *26*, 3395–3407. [CrossRef]
85. Cangussu, N.; Milheiro-Oliveira, P.; Matos, A.M.; Aslani, F.; Maia, L. Comparison of Outlier Detection Approaches for Compressive Strength of Cement-Based Mortars. *J. Build. Eng.* **2024**, *95*, 110276. [CrossRef]
86. *ASTM E178-16a*; Dealing with Outlying Observations. ASTM: West Conshohocken, PA, USA, 2000.
87. *ACI 214R-11*; Guide to Evaluation of Strength Test Results of Concrete. American Concrete Institute (ACI): Farmington Hills, MI, USA, 2011.
88. Duxson, P.; Provis, J.L.; Lukey, G.C.; Mallicoat, S.W.; Kriven, W.M.; Van Deventer, J.S.J. Understanding the Relationship between Geopolymer Composition, Microstructure and Mechanical Properties. *Colloids Surf. A Physicochem. Eng. Asp.* **2005**, *269*, 47–58. [CrossRef]
89. Ji, X.; Wang, Z.; Wang, X.; Zhao, X.; Zhang, H.; Zhang, T. Microstructures and Properties of Alkali-Activated Slags with Composite Activator: Effects of Na_2O Equivalents. *J. Clean. Prod.* **2024**, *450*, 141754. [CrossRef]
90. Mohammed, A.A.; Ahmed, H.U.; Mosavi, A. Survey of Mechanical Properties of Geopolymer Concrete: A Comprehensive Review and Data Analysis. *Materials* **2021**, *14*, 4690. [CrossRef]
91. *ACI 318-19*; Building Code Requirements for Structural Concrete and Commentary. American Concrete Institute (ACI): Farmington Hills, MI, USA, 2019.
92. *AS 3600*; Concrete Structures. Standards Australia: Sydney, Australia, 2018.
93. *EN 1992-1-1*; Eurocode 2: Design of Concrete Structures—Part 1-1: General Rules and Rules for Buildings. British Standard Institution: London, UK, 2004.
94. Dangol, S.; Sirivivatnanon, V.; Shrestha, R.; Gowripalan, N. Development of Geopolymer Concrete for Precast Pipe Application. Doctoral Dissertation, University of Technology Sydney, Sydney, Australia, 2023.

95. Mohyeddin, A.; Karmokar, T.; Fardipour, M. Fracture Energy of Ambient-Cured Fly Ash-Based Geopolymer Concrete. *Aust. J. Struct. Eng.* **2025**, 1–17. [CrossRef]
96. CEB. *fib Model Code for Concrete Structures 2010*; fib: Lausanne, Switzerland, 2013.

Disclaimer/Publisher's Note: The statements, opinions and data contained in all publications are solely those of the individual author(s) and contributor(s) and not of MDPI and/or the editor(s). MDPI and/or the editor(s) disclaim responsibility for any injury to people or property resulting from any ideas, methods, instructions or products referred to in the content.